Resonantly enhanced refractive index without absorption via atomic coherence

M. Fleischhauer, C. H. Keitel, and M. O. Scully
Center for Advanced Studies, University of New Mexico, Albuquerque, New Mexico 87131;
Department of Physics and Astronomy, University of New Mexico, Albuquerque, New Mexico 87131;
and Max-Planck-Institut für Quantenoptik, Garching, Germany W-8046

Chang Su, B. T. Ulrich, and Shi-Yao Zhu
Center for Advanced Studies, University of New Mexico, Albuquerque, New Mexico 87131
and Department of Physics and Astronomy, University of New Mexico, Albuquerque, New Mexico 87131
(Received 13 December 1991)

An enhancement of the index of refraction accompanied by vanishing absorption is shown to be possible in an ensemble of phase-coherent atoms ("phaseonium"). A survey of various possible schemes in which coherence is established by certain coherent or incoherent methods is given, and the main results are compared and contrasted. In particular, the influence of processes such as Doppler broadening that degrade coherence is discussed.

PACS number(s): 42.65.An, 42.50.Md

I. INTRODUCTION

The index of refraction of a gaseous medium at ≈ 1 Torr can reach values as high as 10 or 100 at frequencies near an optical resonance. The price that must be paid for such high dispersion is usually an accompanying high absorption.

However, recently it has been pointed out one way to achieve an ultrahigh index of refraction near an atomic resonance while canceling the absorption. The underlying principles are atomic coherence and quantum interference. These effects are known to cancel absorption at certain frequencies near an atomic resonance, which has led to the observation of nonabsorbing resonances [1,2] and the prediction of lasing without inversion [3–7]. Such a phase-coherent atomic ensemble ("phaseonium") provides us with what is essentially a new state of matter.

In a phaseonium gas without population in the excited level, the absorption cancellation always coincides with vanishing refractivity. However, providing a small fraction of atoms in the excited state, absorption vanishes slightly off resonance, where the real part of the susceptibility has a substantial value. This gives rise to the possibility of high refractivity in a nonabsorbing medium [8–10].

The purpose of the present paper is to give a survey of the various schemes in which atomic coherence and interference effects lead to complete absorption cancellation and an ultrahigh index of refraction. The introduced schemes are compared and contrasted and, in particular, the influence of coherence degrading processes such as Doppler broadening and collisions is studied in all cases.

The linear response of an atomic system on an electric field E is governed by the complex polarization

$$P(z,t)=\epsilon_0\int_{-\infty}^{\infty} d\tau[\chi'(\tau)+i\chi''(\tau)]E(z,t-\tau)\ , \tag{1a}$$

$$P(z,\omega)=\epsilon_0[\chi'(\omega)+i\chi''(\omega)]E(z,\omega)\ , \tag{1b}$$

or more directly by the real (χ') and imaginary (χ'') part of the susceptibility. The relation between the complex susceptibility and the refractive index of the medium is outlined in the Appendix. For an effective two-level medium we have the well-known textbook results [11]:

$$\chi'(\omega)=-\frac{\wp^2 N}{\epsilon_0\hbar}\frac{\Delta}{\Delta^2+\gamma^2}(\rho_{aa}-\rho_{bb})\ , \tag{2a}$$

$$\chi''(\omega)=-\frac{\wp^2 N}{\epsilon_0\hbar}\frac{\gamma}{\Delta^2+\gamma^2}(\rho_{aa}-\rho_{bb})\ , \tag{2b}$$

where Δ is the detuning of the test field with respect to the optical transition, and γ is the decay rate of the atomic coherence. Here, and in the remainder of the paper, $\wp$ is the dipole matrix element of the optical transition, N is the number of atoms per unit volume, and χ' and χ'' are the susceptibilities in frequency space. As can be seen immediately from these equations, a high refractive index is always accompanied either by large absorption or by large gain. In Fig. 1, χ' and χ'' are displayed for a gas of two-level atoms with a number density of 1 atom per cm^3. For the case of a 1 Torr gas ($N=10^{16}/\text{cm}^3$) the maximum value of χ' is therefore approximately 50. However, since χ'' has at the same frequency the same value, an incident light beam would be absorbed in a small fraction of the wavelength. On the other hand, far off resonance, where the gas becomes transparent, a typical value for the real part of the susceptibility is of order 10^{-7} in gases of 1 Torr pressure.

The situation is completely different, however, if multilevel schemes are considered in which atomic coherence is established or quantum interference effects occur: Let us first consider the case of three-level schemes with a pair of closely lying lower or upper levels as shown in Fig. 2. Coherence in this case is established between the doublet states by some external means. Assuming dipole-allowed transitions between the single level and the two closely spaced lower or upper levels [Fig. 2(a) or

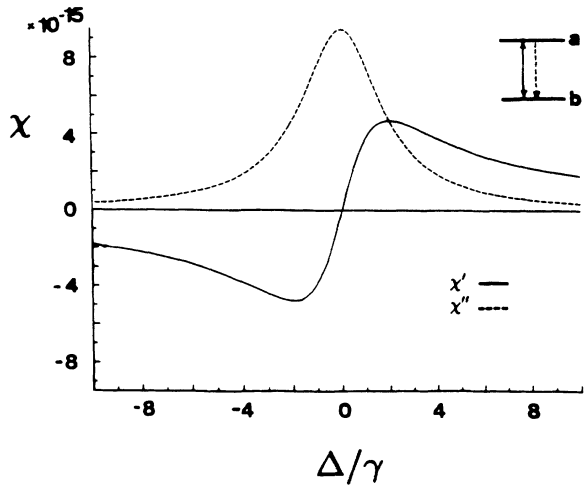

FIG. 1. Real (line) and imaginary (dashed) parts of the linear susceptibility of a gas of two-level atoms with a density of 1 atom per cm^3.

2(b)], the linear susceptibility of the system reads, e.g., in the case of a lower-level pair:

$$\chi=\frac{P}{\epsilon_0 E}=-\left[\frac{\wp N}{\epsilon_0 E}\rho_{ab}+\frac{\wp' N}{\epsilon_0 E}\rho_{ab'}\right] . \tag{3}$$

Here, the nondiagonal matrix elements ρ_{ab} and $\rho_{ab'}$ are determined not only by the population differences, as in the two-level case, but, in addition, by new terms $\rho_{bb'}$ and $\rho_{b'b}$ which express the coherence between the two close levels

$$\dot{\rho}_{ab}=-(i\Delta+\gamma_{ab})\rho_{ab}-\frac{i\wp E}{\hbar}(\rho_{bb}-\rho_{aa})-\frac{i\wp' E}{\hbar}\rho_{b'b} , \tag{4a}$$

$$\dot{\rho}_{ab'}=-(i\Delta+\gamma_{ab'})\rho_{ab'}-\frac{i\wp' E}{\hbar}(\rho_{b'b'}-\rho_{aa})-\frac{i\wp E}{\hbar}\rho_{bb'} . \tag{4b}$$

In contrast to the two-level case, these extra terms may cancel the absorption terms proportional to lower-level populations. Hence this low-frequency coherence may lead to nonabsorbing resonances or lasing without inversion [5]. In the case of zero population in the upper level at the point of vanishing absorption, this may lead to a vanishing refractive index with a large slope [3,4,9]. However, by providing a relatively small population in the excited state, not only the derivative but also the index of refraction itself can be large at frequencies where $\mathrm{Im}P=0$ [8–10].

The origin of this behavior is quantum interference. This can be seen most easily if we consider the total probability of emitting or absorbing a photon, for instance, for the case shown in Fig. 2(a). Given an initial state

$$|\psi(0)\rangle=a(0)|a\rangle+b(0)|b\rangle+b'(0)|b'\rangle ,$$

the probability of emission is the sum of the transition probabilities to b and b', that is

$$\begin{aligned}P_{\mathrm{em}}&=\{\cdots\}\{|\wp_{ab}|^2|a(0)|^2+|\wp_{ab'}|^2|a(0)|^2\}\\&=\{\cdots\}|\wp|^2 2\rho_{aa}(0) .\end{aligned} \tag{5a}$$

The probability of absorption of an atom in the lower states b and b' to the upper level a is the modulus squared of the sum of the transition amplitudes:

$$\begin{aligned}P_{\mathrm{abs}}&=\{\cdots\}\{|\wp_{ab}b(0)+\wp_{ab'}b'(0)|^2\}\\&=\{\cdots\}|\wp|^2\{\rho_{bb}(0)+\rho_{b'b'}(0)+\rho_{bb'}(0)+\rho_{b'b}(0)\} ,\end{aligned} \tag{5b}$$

where we have taken the case $\wp_{ab}=\wp_{ab'}=\wp$, and $\{\cdots\}$ is an uninteresting prefactor which contains the intensity of the radiation field. The last two terms in Eq. (5b) are the interference contributions to this total probability. They need not be positive and in fact may cancel the first two terms for a certain frequency.

From the point of view of quantum interferences, it is near at hand to extend the consideration to other schemes in which similar interference effects occur: If the lower or upper level of a single dipole-allowed transition is strongly coupled to another level, as indicated in Fig. 3, absorption and/or emission may occur via different pathways, either directly or via the auxiliary level c. The contributions from the different pathways to the total absorption or emission probability then lead to similar interference terms, as in Eq. (5b). Both types of interference effects may lead to transparent materials with a high index of refraction and will be discussed in this paper.

In order to outline the principle mechanisms that lead to a high-index material, we discuss in Sec. II, in detail, a three-level system with a lower-level doublet in which coherence is established by preparing the atoms in a

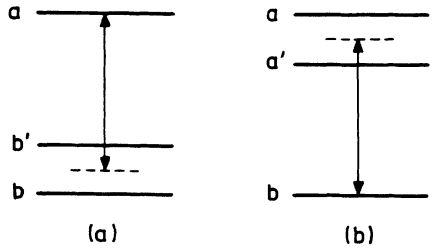

FIG. 2. In contrast to a two-level system, the linear-optical properties of a three-level system with two closely spaced (a) lower or (b) upper levels are strongly influenced by the coherence between the level doublet.

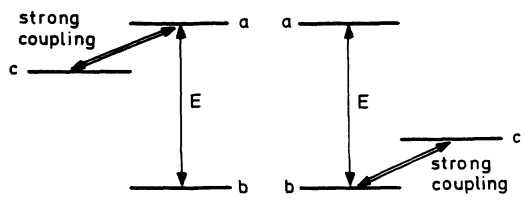

FIG. 3. A strong coupling of the upper or lower level of a single optical transition to an auxiliary level c via an intense driving field creates interferences between different absorption and/or emission pathways.

coherent superposition via pulse excitation [8].

There are several ways of creating coherence or quantum interference in atomic systems. The most common technique is to use coherent fields driving two levels either directly or via a Raman-type transition to another auxiliary level. The features of different coherently driven systems are compared and contrasted in Sec. III. In addition to these coherent techniques, coherence or interference can also be established by incoherent methods, which we discuss in Sec. IV. In Sec. V we propose several atomic schemes for a practical implementation of the index-enhancement effect. The influence of several coherence degrading processes, such as Doppler broadening, are discussed in some numerical examples for all the schemes investigated.

II. INDEX ENHANCEMENT IN A MEDIUM WITH INITIAL ATOMIC COHERENCE

To illustrate the basic mechanism by which coherence influences the refractive index and absorption, we consider a simple model in which gas atoms are initially prepared in a coherent superposition of the two lower levels b and b'. This can be accomplished, for example, by coherent pulse excitation, as described in Fig. 4.

For such coherent preparation, the initial condition on the density matrix for the ith atom is

$$\rho^i=\begin{bmatrix}\rho^0_{aa} & 0 & 0\\ 0 & \rho^0_{b'b'} & \rho^0_{b'b}\\ 0 & \rho^0_{bb'} & \rho^0_{bb}\end{bmatrix}.$$

The atoms are injected at a rate r, so that the time evolution for the macroscopic density matrix, introduced in Ref. 11, is then determined by

$$\dot\rho_{ab'}=-(i\Delta_{ab'}+\gamma_{ab'})\rho_{ab'}-\frac{i}{\hbar}\not{\mu}'(\rho_{b'b'}-\rho_{aa})E-\frac{i}{\hbar}\not{\mu}\rho_{bb'}E\ , \tag{6a}$$

$$\dot\rho_{ab}=-(i\Delta_{ab}+\gamma_{ab})\rho_{ab}-\frac{i}{\hbar}\not{\mu}(\rho_{bb}-\rho_{aa})E-\frac{i}{\hbar}\not{\mu}'\rho_{b'b}E\ , \tag{6b}$$

$$\dot\rho_{b'b}=r\rho^0_{b'b}-(i\omega_{b'b}+\gamma_{b'b})\rho_{b'b}-\frac{i}{\hbar}(\not{\mu}'\rho_{ab}E^*-\not{\mu}\rho_{b'a}E)\ , \tag{6c}$$

$$\dot\rho_{aa}=r\rho^0_{aa}-\gamma_a\rho_{aa}-\frac{i}{\hbar}[(\not{\mu}'\rho_{b'a}+\not{\mu}\rho_{ba})E-\text{c.c.}]\ , \tag{6d}$$

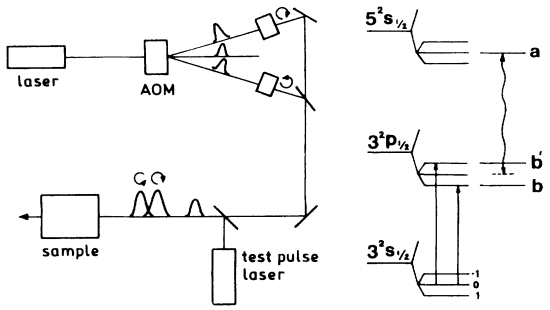

FIG. 4. A possible experimental setup to establish atomic coherence via pulse excitation in Na. A strong linear polarized pump pulse is split into three parts with slightly different frequencies by an acousto-optical modulator (AOM). Two polarizers generate circular polarization in order to pump the $\Delta m=\pm1$ transitions as indicated on the right side of the figure. The time delay of the two pump pulses is chosen to adjust the right phase ϕ in Eq. (9).

$$\dot\rho_{b'b'}=r\rho^0_{b'b'}-\gamma_{b'}\rho_{b'b'}-\frac{i}{\hbar}(\not{\mu}'\rho_{ab'}E^*-\text{c.c.})\ , \tag{6e}$$

$$\dot\rho_{bb}=r\rho^0_{bb}-\gamma_b\rho_{bb}-\frac{i}{\hbar}(\not{\mu}'\rho_{ab}E^*-\text{c.c.})\ , \tag{6f}$$

where in the conventional notation, $\gamma_{\alpha\beta}=(\gamma_\alpha+\gamma_\beta)/2+\gamma_{\text{phase}}$, and we have introduced a rotating frame. Here $\Delta_{\alpha\beta}=\omega_{\alpha\beta}-\nu$, where the test field has a frequency ν and a slowly varying amplitude E.

Next we let the system go to steady state, in which case,

$$\rho_{ab'}=\frac{i}{\hbar}E\frac{1}{\gamma_{ab'}+i\Delta_{ab'}}[\not{\mu}'(\rho_{aa}-\rho_{b'b'})-\not{\mu}\rho_{bb'}]\ , \tag{7a}$$

$$\rho_{ab}=\frac{i}{\hbar}E\frac{1}{\gamma_{ab}+i\Delta_{ab}}[\not{\mu}(\rho_{aa}-\rho_{bb})-\not{\mu}'\rho_{b'b}]\ . \tag{7b}$$

For a first-order analysis in the laser field E, we insert the zeroth-order values of ρ_{aa}, $\rho_{b'b'}$, ρ_{bb}, and $\rho_{bb'}$,

$$\rho^{(0)}_{\alpha\alpha}=\frac{r\rho^0_{\alpha\alpha}}{\gamma_\alpha}\quad(\alpha=a,b,b')\ , \tag{8a}$$

$$\rho^{(0)}_{b'b}=\frac{r\rho^0_{b'b}}{i\omega_{b'b}+\gamma_{b'b}} \tag{8b}$$

into above Eqs. (7a) and (7b). Finally, we substitute these into Eq. (3) and obtain

$$\chi'=\frac{\not{\mu}^2 r}{\hbar\epsilon_0 V}\left\{\frac{1}{\gamma^2_{ab'}+\Delta^2_{ab'}}\left[\Delta_{ab'}\left[\frac{\rho^0_{aa}}{\gamma_a}-\frac{\rho^0_{b'b'}}{\gamma_{b'}}\right]-\frac{|\rho^0_{b'b}|}{(\gamma^2_{b'b}+\omega^2_{b'b})^{1/2}}(\Delta_{ab'}\cos\phi+\gamma_{ab'}\sin\phi)\right]\right.$$
$$\left.+\frac{1}{\gamma^2_{ab}+\Delta^2_{ab}}\left[\Delta_{ab}\left[\frac{\rho^0_{aa}}{\gamma_a}-\frac{\rho^0_{bb}}{\gamma_b}\right]-\frac{|\rho^0_{b'b}|}{(\gamma^2_{b'b}+\omega^2_{b'b})^{1/2}}(\Delta_{ab}\cos\phi-\gamma_{ab}\sin\phi)\right]\right\}, \tag{9a}$$

$$\chi''=\frac{\not{\mu}^2 r}{\hbar\epsilon_0 V}\left\{\frac{1}{\gamma^2_{ab'}+\Delta^2_{ab'}}\left[\gamma_{ab'}\left[\frac{\rho^0_{aa}}{\gamma_a}-\frac{\rho^0_{b'b'}}{\gamma_{b'}}\right]-\frac{|\rho^0_{b'b}|}{(\gamma^2_{b'b}+\omega^2_{b'b})^{1/2}}(\gamma_{ab'}\cos\phi-\Delta_{ab'}\sin\phi)\right]\right.$$
$$\left.+\frac{1}{\gamma^2_{ab}+\Delta^2_{ab}}\left[\gamma_{ab}\left[\frac{\rho^0_{aa}}{\gamma_a}-\frac{\rho^0_{bb}}{\gamma_b}\right]-\frac{|\rho^0_{b'b}|}{(\gamma^2_{b'b}+\omega^2_{b'b})^{1/2}}(\gamma_{ab}\cos\phi+\Delta_{ab}\sin\phi)\right]\right\}, \tag{9b}$$

where V is the interaction volume. The phase ϕ is defined by

$$\frac{\mathcal{K}'\mathcal{K}\rho^0_{b'b}}{\gamma_{b'b}+i\omega_{b'b}}=\frac{\mathcal{K}^2|\rho^0_{b'b}|e^{i\phi}}{(\gamma^2_{b'b}+\omega^2_{b'b})^{1/2}},$$

and, for simplicity, we have taken $\mathcal{K}'=\mathcal{K}$.

From Eqs. (9a) and (9b), we can see that it is possible to make the absorption (χ'') vanish, while maintaining a large refractive index (χ'). We define $\Delta=(\Delta_{ab}+\Delta_{ab'})/2$ and adjust $\omega_{b'b}$ by means of a dc magnetic field, so that $\omega_{b'b}=\gamma_{b'b}$, and consider the physically reasonable case $\gamma_b=\gamma_{b'}$. Finally, we prepare the levels b' and b coherently, so that $\phi=5\pi/4$ and $\rho^0_{bb}=\rho^0_{b'b}=|\rho^0_{b'b}|$. The resulting polarization is plotted in Fig. 5 [12]. It can be seen that a high index of refraction can be obtained with zero absorption.

Next we consider the case in which all of the above conditions are met but now, in addition, $\gamma_a=\gamma_b=\gamma_{b'}=\gamma$. Then, when $\Delta\cong 1.1\gamma$ and a few percent of the atoms are in the a state, the absorption vanishes, while the dispersive part of the susceptibility is of order

$$\chi'\approx\frac{1}{10}\frac{\mathcal{K}^2N_a}{\hbar\epsilon_0\gamma}, \tag{10}$$

where $N_a=r\rho^0_{aa}/V\gamma$ is the a-state atomic density. Equation (10) may be written in terms of the radiative decay rate $\gamma_r=\mathcal{K}^2\nu^3/6\pi\hbar\epsilon_0c^3$ as

$$\chi'\approx\frac{1}{10}\frac{3\lambda^3}{4\pi^2}\frac{\gamma_r}{\gamma}N_a. \tag{11}$$

Thus we realize that a large index of refraction is achievable in a transparent medium. If we consider, for instance, the case of $N_a=10^{11}$ cm^{-3} (a gas of 1 mtorr pressure at room temperature with 1% of the atoms in the excited state has the same density of excited atoms) and assume purely radiative decay ($\gamma_r=\gamma$), we have $\chi'\approx 7\times10^{-4}$ for $\lambda=1$ μm at a point of complete transparency. This is by three orders of magnitude larger than the value achievable in usual transparent gases of this pressure. By increasing the density of atoms, much larger values of χ' are possible. Note, however, that then the gas has to be cooled in order to keep collisional broadening small so that $\gamma\sim\gamma_r$.

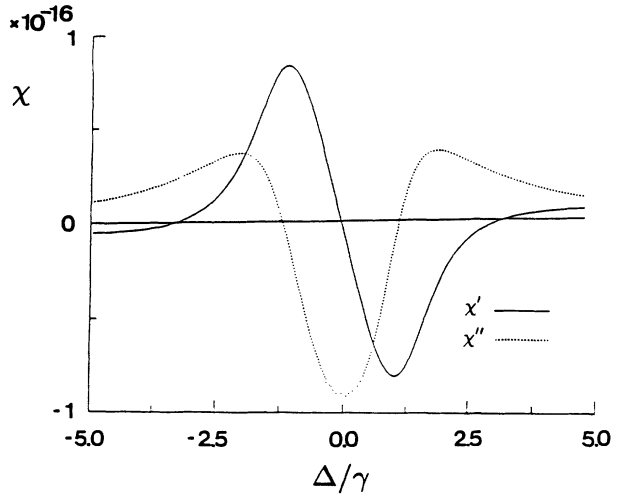

FIG. 5. Real (line) and imaginary (dashed) parts of the susceptibility as a function of the detuning Δ for the case of injected atomic coherence. We have assumed purely radiative decay. One percent of the atoms are initially in the excited state and $\gamma_a=0.1\gamma_b$.

In the following two sections we discuss methods to generate coherence via coherent microwave and Raman fields and by incoherent means. Instead of injecting atoms prepared in an initial coherent state, in the following sections the coherence or interferences are maintained by coherent or incoherent fields applied simultaneously with the test field for which the index of refraction is modified.

III. HIGH INDEX OF REFRACTION IN COHERENTLY DRIVEN SCHEMES

The most common technique used to establish a steady-state atomic coherence or interference of pathways, which can lead to transparent high index materials, is the application of strong coherent driving fields. Examples such as microwave driving of the level doublet or Raman driving of these levels via an additional auxiliary level have been discussed in the study of lasing without inversion [3–7]. In this section we demonstrate that these schemes provide transparent materials with very high refractivity. Since the analysis is straightforward, we restrict ourselves, however, to presenting and discussing the main results.

A simple way of establishing the lower-level coherence in the Λ quantum-beam configuration in a different way from that discussed in the preceding section is the application of a microwave field in two-photon resonance of the lower-level doublet as indicated in Fig. 6. For the present, however, we exclude this scheme from the discussion because it cannot be treated within a simple steady-state analysis of the density-matrix equations. To calculate the linear-optical properties of this scheme, unitary transformation techniques may be applied [5].

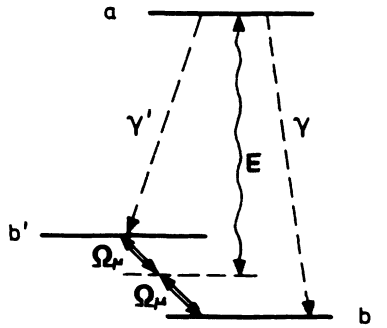

FIG. 6. A strong microwave field in two-photon resonance with the two lower levels of a Λ-quantum beat scheme produces coherence between these levels.

A. Raman-driven scheme

Instead of creating the coherence between the two closely spaced levels via a direct coherent two-photon transition, we now present a different possibility in which an applied coherent field couples the two lower levels via an additional auxiliary level. According to Fig. 7, the lower-level doublet b-b' couples to the auxiliary level c and thus to itself via a coherent field with Rabi frequency Ω_R for the b-c and Ω'_R for the b'-c transition. Both transitions a-b and a-b' are assumed to be dipole allowed and to interact with the test field E. Defining the dipole-matrix elements of the two transitions as $\wp$ and $\wp'$, the density-matrix equations read in a rotating frame

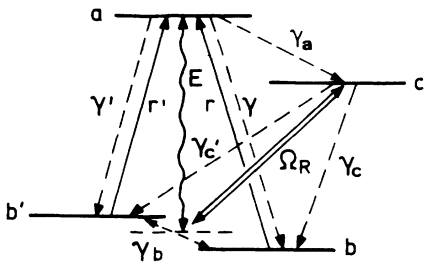

FIG. 7. Level scheme for the Raman-driven case. The two dipole-allowed transitions a-b and a-b' are coupled to a single mode test field E. Both lower levels are driven to a fourth auxiliary level via a strong Raman field with Rabi frequency Ω_R.

$$\dot{\rho}_{aa}=-(\gamma+\gamma'+\gamma_a)\rho_{aa}+r\rho_{bb}+r'\rho_{b'b'}+i\left[\frac{\wp}{\hbar}E^*\rho_{ab}+\frac{\wp'}{\hbar}E^*\rho_{ab'}-\text{c.c.}\right], \tag{12a}$$

$$\dot{\rho}_{b'b'}=-(\gamma'_b+r')\rho_{b'b'}+\gamma_b\rho_{bb}+\gamma'\rho_{aa}+\gamma'_c\rho_{cc}+i\left[\frac{\wp'}{\hbar}E\rho_{b'a}+\Omega'_R\rho_{b'c}-\text{c.c.}\right], \tag{12b}$$

$$\dot{\rho}_{bb}=-(\gamma_b+r)\rho_{bb}+\gamma'_b\rho_{b'b'}+\gamma\rho_{aa}+\gamma_c\rho_{cc}+i\left[\frac{\wp}{\hbar}E\rho_{ba}+\Omega_R\rho_{bc}-\text{c.c.}\right], \tag{12c}$$

$$\dot{\rho}_{cc}=-(\gamma_c+\gamma'_c)\rho_{cc}+\gamma_a\rho_{aa}+i(\Omega'^*_R\rho_{cb'}+\Omega^*_R\rho_{cb}-\text{c.c.}), \tag{12d}$$

$$\dot{\rho}_{ab'}=-(\gamma_{ab'}+i\Delta_{ab'})\rho_{ab'}+i\left[\frac{\wp'}{\hbar}E(\rho_{aa}-\rho_{b'b'})-\frac{\wp}{\hbar}E\rho_{bb'}+\Omega'_R\rho_{ac}\right], \tag{12e}$$

$$\dot{\rho}_{ab}=-(\gamma_{ab}+i\Delta_{ab})\rho_{ab}+i\left[\frac{\wp}{\hbar}E(\rho_{aa}-\rho_{bb})-\frac{\wp'}{\hbar}E\rho_{b'b}+\Omega_R\rho_{ac}\right], \tag{12f}$$

$$\dot{\rho}_{b'b}=-[\gamma_{b'b}+i(\Delta_{ab}-\Delta_{ab'})]\rho_{b'b}+i\left[\frac{\wp}{\hbar}E\rho_{b'a}-\frac{\wp'}{\hbar}E^*\rho_{ab}+\Omega_R\rho_{b'c}-\Omega'^*_R\rho_{cb}\right], \tag{12g}$$

$$\dot{\rho}_{cb'}=-(\gamma_{cb'}+i\Delta'_R)\rho_{cb'}+i\left[\Omega'_R(\rho_{cc}-\rho_{b'b'})-\Omega_R\rho_{bb'}+\frac{\wp'}{\hbar}E\rho_{ca}\right], \tag{12h}$$

$$\dot{\rho}_{cb}=-(\gamma_{cb}+i\Delta_R)\rho_{cb}+i\left[\Omega_R(\rho_{cc}-\rho_{bb})-\Omega'_R\rho_{b'b}+\frac{\wp}{\hbar}E\rho_{ca}\right], \tag{12i}$$

$$\dot{\rho}_{ac}=-[\gamma_{ac}+i(\Delta_{ab}-\Delta_R)]\rho_{ac}-i\left[\frac{\wp}{\hbar}E\rho_{bc}+\frac{\wp'}{\hbar}E\rho_{b'c}-\Omega^*_R\rho_{ab}-\Omega'^*_R\rho_{ab'}\right]. \tag{12j}$$

Here we have introduced the detunings of the test field with respect to the two affected transitions as $\Delta_{ab}=\omega_{ab}-\nu$ and $\Delta_{ab'}=\omega_{ab'}-\nu$. The detunings of the Raman field with respect to the two Raman transitions are $\Delta_R=\omega_{cb}-\nu_R$ and $\Delta'_R=\omega_{cb'}-\nu_R$. Moreover, pump processes are included, since for the purpose of high refractivity at a point of vanishing absorption some population in the upper lasing level is necessary. As a consequence of the complicated four-level structure, the general result for the linear susceptibility cannot be given here in a simple compact form. The Raman scheme, however, has so far turned out to be the most favorable case for experimental implementation. For this reason we consider it worthwhile to present the complex susceptibility of this scheme in its full generality:

$$\begin{aligned}\chi=\frac{N}{\epsilon_0\hbar}\Bigg\{&\frac{i(1+y)\wp}{(1+x+y)\Gamma_{ab}}[\wp(\rho^{(0)}_{aa}-\rho^{(0)}_{bb})-\wp'\rho^{(0)}_{b'b}]-\frac{i\Omega_R\Omega'^*_R}{(1+x+y)\Gamma_{ac}\Gamma_{ab}\Gamma_{ab'}}[\wp'(\rho^{(0)}_{aa}-\rho^{(0)}_{b'b'})-\wp\rho^{(0)}_{bb'}]\\&+\frac{\Omega_R}{(1+x+y)\Gamma_{ab}\Gamma_{ac}}[\wp\rho^{(0)}_{bc}+\wp'\rho^{(0)}_{b'c}]+\frac{i(1+x)\wp'}{(1+x+y)\Gamma_{ab'}}[\wp'(\rho^{(0)}_{aa}-\rho^{(0)}_{b'b'})-\wp\rho^{(0)}_{bb'}]\\&-\frac{i\Omega^*_R\Omega'_R}{(1+x+y)\Gamma_{ac}\Gamma_{ab}\Gamma_{ab'}}[\wp(\rho^{(0)}_{aa}-\rho^{(0)}_{bb})-\wp'\rho^{(0)}_{b'b}]+\frac{\Omega'_R}{(1+x+y)\Gamma_{ac}\Gamma_{ab'}}[\wp\rho^{(0)}_{bc}+\wp'\rho^{(0)}_{b'c}]\Bigg\},\end{aligned} \tag{13}$$

with the following abbreviations:

$$x=\frac{|\Omega_R|^2}{\Gamma_{ab}\Gamma_{ac}},\quad y=\frac{|\Omega_R'|^2}{\Gamma_{ab'}\Gamma_{ac}}$$

and

$$\Gamma_{ab}=\gamma_{ab}+i\Delta_{ab},\quad \Gamma_{ab'}=\gamma_{ab'}+i\Delta_{ab'},$$

$$\Gamma_{cb}=\gamma_{bc}+i\Delta_R,\quad \Gamma_{cb'}=\gamma_{b'c}+i\Delta_R',$$

$$\Gamma_{b'b}=\gamma_{b'b}+i(\Delta_{ab}-\Delta_{ab'}),\quad \Gamma_{ac}=\gamma_{ac}+i(\Delta_{ab}-\Delta_R).$$

The zeroth-order solutions $\rho^0_{\alpha\beta}$ in Eq. (13) are

$$\rho_{bb}^{(0)}=-\frac{A_1B_2+A_2B_1}{Z},\tag{14a}$$

$$\rho_{b'b'}^{(0)}=-\frac{A_2C_1+A_1C_2}{Z},\tag{14b}$$

$$\rho_{cc}^{(0)}=\frac{B_1C_2-B_2C_1}{Z},\tag{14c}$$

$$\rho_{bc}^{(0)}=-i\Omega_R^*\frac{(1+x_1)(\rho_{cc}^{(0)}-\rho_{bb}^{(0)})-y_1(\Gamma_{cb}/\Gamma_{cb'}^*)(\rho_{cc}^{(0)}-\rho_{b'b'}^{(0)})}{\Gamma_{cb}(1+x_1+y_1)},\tag{14d}$$

$$\rho_{b'c}^{(0)}=-i\Omega_R'^*\frac{(1+y_1^*)(\rho_{cc}^{(0)}-\rho_{b'b'}^{(0)})-x_1^*(\Gamma_{cb'}/\Gamma_{cb}^*)(\rho_{cc}^{(0)}-\rho_{bb}^{(0)})}{\Gamma_{cb'}(1+x_1^*+y_1^*)},\tag{14e}$$

$$\rho_{b'b}^{(0)}=\Omega_R^*\Omega_R'\frac{(1/\Gamma_{cb})(\rho_{cc}^{(0)}-\rho_{bb}^{(0)})+(1/\Gamma_{cb'}^*)(\rho_{cc}^{(0)}-\rho_{bb}^{(0)})}{\Gamma_{b'b}(1+x_1+y_1)},\tag{14f}$$

with the parameters used above defined as

$$Z=B_1C_2-A_1B_2D_2-A_2C_1D_1-B_2C_1-A_1C_2D_1-A_2B_1D_2,$$

$$A_1=1+a+a^*-b-b^*,\quad D_1=1+\frac{r'}{\gamma'+\gamma+\gamma_a},$$

$$A_2=1+c+c^*-d-d^*,\quad D_2=1+\frac{r}{\gamma'+\gamma+\gamma_a},$$

$$B_1=\frac{\gamma_b'}{\gamma_c}+\frac{r'/\gamma_c}{1+(\gamma'+\gamma_a)/\gamma}+b+b^*,$$

$$B_2=\frac{\gamma_b'}{\gamma_c'}+\frac{r'(\gamma+\gamma_a)/\gamma_c'\gamma'}{1+(\gamma+\gamma_a)/\gamma'}+c+c^*,$$

$$C_1=\frac{\gamma_b}{\gamma_c}+\frac{r(\gamma'+\gamma_a)/\gamma_c\gamma}{1+(\gamma'+\gamma_a)/\gamma}+a+a^*,$$

$$C_2=\frac{\gamma_b}{\gamma_c'}+\frac{r/\gamma_c'}{1+(\gamma+\gamma_a)/\gamma'}+d+d^*,$$

and

$$a=\frac{|\Omega_R|^2(1+x_1)}{\gamma_c\Gamma_{cb}(1+x_1+y_1)},\quad c=\frac{|\Omega_R'|^2(1+y_1)}{\gamma_c'\Gamma_{cb'}^*(1+x_1+y_1)},$$

$$b=\frac{x_1y_1\Gamma_{b'b}}{\gamma_c(1+x_1+y_1)},\quad d=\frac{x_1y_1\Gamma_{b'b}}{\gamma_c'(1+x_1+y_1)},$$

$$x_1=\frac{|\Omega_R|^2}{\Gamma_{cb'}^*\Gamma_{b'b}},\quad y_1=\frac{|\Omega_R'|^2}{\Gamma_{cb}\Gamma_{b'b}}.$$

In Fig. 8 the real and imaginary parts of the susceptibility are depicted as a function of the detuning $\Delta=(\Delta_{ab}+\Delta_{ab'})/2$ of the field with respect to the midfrequency of the two optical transitions. The possibility of a large refractive index at a point with vanishing imaginary part of the polarization becomes evident here.

In the case when the Raman and the test field have the same propagation direction, the corresponding transitions experience a Doppler shift in the same direction. As a consequence the Raman-driven scheme is less sensi-

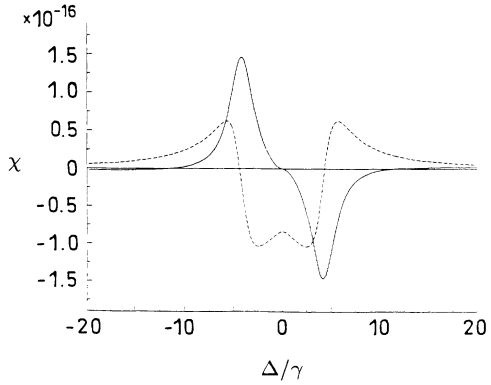

FIG. 8. Real (line) and imaginary (dashed) parts of the linear susceptibility for the Raman scheme. The level spacing between the two close lower levels is equal to $\gamma=\gamma'$. The Rabi frequency Ω_R is 3γ and the pump and decay rates $r=r=0.2\gamma$. $\gamma_c=\gamma_c'=\gamma$, $\gamma_a=10^{-3}\gamma$. The decay rate between the lower levels is assumed to be small ($\gamma_b=\gamma_{b'}=10^{-3}\gamma$).

tive to Doppler broadening. Figure 9 displays the influence of an atomic velocity distribution on the real and imaginary parts of the susceptibility for a test-field frequency which is twice as high as the Raman frequency. For a Doppler width of 20γ, where γ is the radiative decay rate of the test-field transition, the achievable value of χ' diminishes only by a factor of $\frac{1}{2}$ compared to the Doppler-free case.

All systems discussed in the following sections provide a high refractive index accompanied by perfect transparency only for a very narrow frequency region. Furthermore, in all schemes for certain frequencies, the system shows gain because of the upper-level population. It is worth noting, however, that in the Raman scheme we can even have a large refractive index with high transparency of the medium in a broad spectral region, as is clear from Fig. 10. The separation of the two absorption peaks increases thereby with the splitting between the two lower levels b and b' and the Rabi frequency Ω_R of the Raman field. Their heights, and therefore the maximum value of χ', diminish with increasing peak separation. Moreover, although a few percent of the atoms are in the upper lasing level, in this particular case, there is no gain for any frequency value. In this parameter regime the system is more sensitive to Doppler broadening

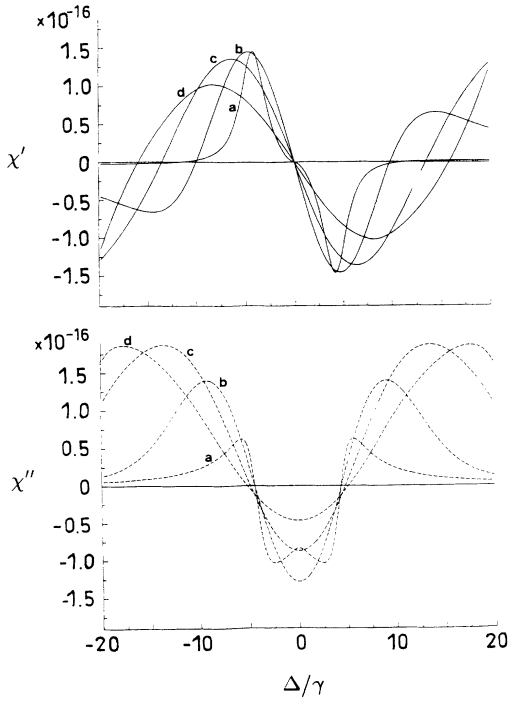

FIG. 9. Influence of Doppler broadening on the real (upper curves) and imaginary (lower curves) parts of χ for the case of parallel propagating Raman and test field. The Raman field frequency here is assumed to be half the test-field frequency. Because the test as well as the Raman fields experience a Doppler shift in the same direction, this scheme is much less sensitive to Doppler broadening than the following schemes. The values of the Dopplerwidth are (a) 0, (b) 5γ, (c) 10γ, and (d) 20γ. All other parameters are same as in Fig. 8.

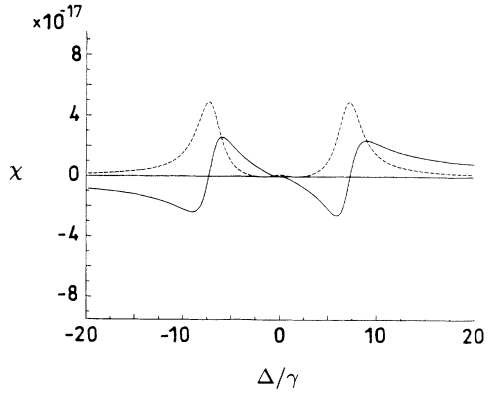

FIG. 10. χ' (line) and χ'' (dashed) as function of Δ for the Raman scheme for $\omega_{b'b}=\gamma$, $r=r=0.017\gamma$, and $\Omega_R=5\gamma$. The other parameters are same as in Fig. 8. Whereas in the other schemes a high refractive index accompanied by small or even vanishing absorption is possible only for a small frequency region, here we can have a broad band effect. Moreover it is evident that there is no frequency region in which the system shows gain.

than in the previous case (cf. Fig. 11). For appropriately large Ω_R, however, this influence can be rendered small.

B. Upper-level microwave scheme

Here we consider the case depicted in Fig. 12. Two levels a and b are coupled via an allowed dipole transition to the test field E. The upper level is also coupled to a third level c via a strong microwave field of Raby frequency Ω_μ. This coupling gives rise to interference of

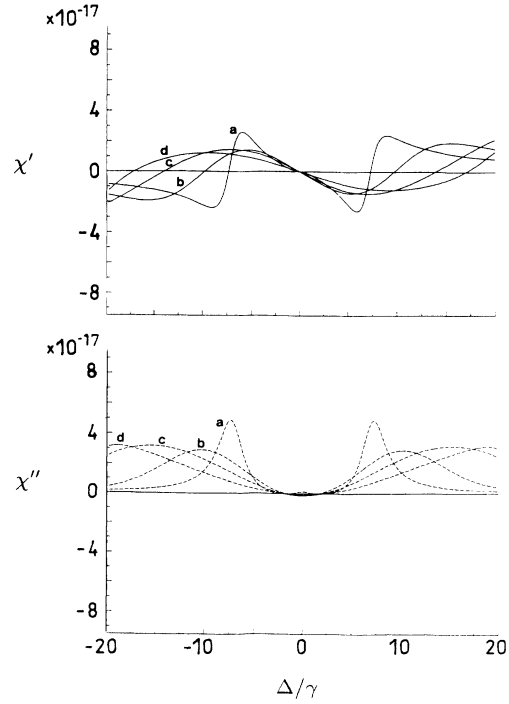

FIG. 11. Influence of Doppler broadening on χ' (upper curves) and χ'' in the Raman scheme for the parameters chosen in Fig. 10.

different possible pathways of absorption in the same order in the test field. To achieve a high refractive index, we need some population in the upper level of the optical transition. Hence we include (indirect) pump mechanisms as depicted in Fig. 12. The complete set of density-matrix equations for this scheme then reads in a rotating frame:

$$\dot{\rho}_{aa} = -(\gamma + r_\mu)\rho_{aa} + r\rho_{bb} + \gamma_\mu \rho_{cc} - i\left[\frac{\wp E}{\hbar}\rho_{ba} + \Omega_\mu^* \rho_{ca} - \text{c.c.}\right], \tag{15a}$$

$$\dot{\rho}_{bb} = -(r + r_c)\rho_{bb} + \gamma\rho_{aa} + \gamma_c \rho_{cc} + i\left[\frac{\wp E}{\hbar}\rho_{ba} - \frac{\wp E^*}{\hbar}\rho_{ab}\right], \tag{15b}$$

$$\dot{\rho}_{cc} = -(\gamma_c + \gamma_\mu)\rho_{cc} + r_c\rho_{bb} + r_\mu\rho_{aa} + i(\Omega_\mu^*\rho_{ca} - \Omega_\mu\rho_{ac}), \tag{15c}$$

$$\dot{\rho}_{ab} = -(i\Delta + \gamma_{ab})\rho_{ab} + i\frac{\wp E}{\hbar}(\rho_{aa} - \rho_{bb}) - i\Omega_\mu^*\rho_{cb}, \tag{15d}$$

$$\dot{\rho}_{cb} = -[i(\Delta + \Delta_\mu) + \gamma_{cb}]\rho_{cb} - i\Omega_\mu\rho_{ab} + i\frac{\wp E}{\hbar}\rho_{ca}, \tag{15e}$$

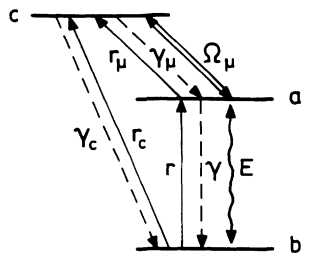

FIG. 12. Level scheme for the upper-level microwave scheme. The transition from a to b is of optical frequency and couples to the test field E. Level a is coupled to a third level c via a strong microwave field of Rabi frequency Ω_μ.

$$\dot{\rho}_{ca} = -(i\Delta_\mu + \gamma_{ca})\rho_{ca} + i\Omega_\mu(\rho_{cc} - \rho_{aa}) + i\frac{\wp E^*}{\hbar}\rho_{cb}. \tag{15f}$$

The quantities Δ and Δ_μ denote the detuning of the test and the microwave field with respect to the corresponding transitions ($\Delta = \omega_{ab} - \nu, \Delta_\mu = \omega_{ca} - \nu_\mu$), and $\gamma_{\alpha\beta}$ are the decay rates of the coherences $\rho_{\alpha\beta}$. Solving for the steady state to first order in the test field E leads to the following general solution for the real and imaginary parts of the polarization:

$$\chi' = \frac{N\wp^2}{\epsilon_0\hbar DD^*}\frac{1}{M}\left[-(|\Omega_\mu|^2 - \Delta^2 - \Delta\Delta_\mu + \gamma_{ab}\gamma_{cb})\left\{(\Delta+\Delta_\mu)[(\gamma - r - r_c)(\gamma_c + \gamma_\mu + K_\mu) + \gamma_c(r_\mu + r_c + K_\mu)] - \frac{1}{2}K_\mu\frac{\Delta_\mu}{\gamma_{ca}}[r(\gamma_\mu + \gamma_c - r_\mu) + r_c(\gamma_\mu - r_\mu - \gamma)]\right\} + [\Delta\gamma_{cb} + (\Delta+\Delta_\mu)\gamma_{ab}]\{\gamma_{cb}[(\gamma - r - r_c)(\gamma_c + \gamma_\mu + K_\mu) + \gamma_c(r_\mu + r_c + K_\mu)] + \tfrac{1}{2}K_\mu[r(\gamma_\mu + \gamma_c - r_\mu) + r_c(\gamma_\mu - r_\mu - \gamma)]\}\right], \tag{16a}$$

$$\chi'' = \frac{N\wp^2}{\epsilon_0\hbar DD^*}\frac{1}{M}\left[(|\Omega_\mu|^2 - \Delta^2 - \Delta\Delta_\mu + \gamma_{ab}\gamma_{cb})\{\gamma_{cb}[(\gamma - r - r_c)(\gamma_c + \gamma_\mu + K_\mu) + \gamma_c(r_\mu + r_c + K_\mu)] + \tfrac{1}{2}K_\mu[r(\gamma_\mu + \gamma_c - r_\mu) + r_c(\gamma_\mu - r_\mu - \gamma)]\} + [\Delta\gamma_{cb} + (\Delta+\Delta_\mu)\gamma_{ab}]\left\{(\Delta+\Delta_\mu)[(\gamma - r - r_c)(\gamma_c + \gamma_\mu + K_\mu) + \gamma_c(r_\mu + r_c + K_\mu)] - \frac{1}{2}K_\mu\frac{\Delta_\mu}{\gamma_{ca}}[r(\gamma_\mu + \gamma_c - r_\mu) + r_c(\gamma_\mu - r_\mu - \gamma)]\right\}\right]. \tag{16b}$$

Here N stands for the total number of atoms per volume in the sample and, furthermore, we have defined

$$D = (|\Omega_\mu|^2 - \Delta^2 - \Delta\Delta_\mu + \gamma_{ab}\gamma_{cb}) + i[\Delta\gamma_{cb} + (\Delta+\Delta_\mu)\gamma_{ab}], \tag{17}$$

$$M = (\gamma_c + \gamma_\mu + K_\mu)(\gamma + r_c + r) + (r_\mu + K_\mu)(\gamma_c + r_c + r) + r_c(\gamma - \gamma_c), \tag{18}$$

and

$$K_\mu = \frac{2\gamma_{ca}|\Omega_\mu|^2}{\Delta_\mu^2 + \gamma_{ca}^2}. \tag{19}$$

To obtain physical insight into these solutions, we make some reasonable simplifying assumptions. Since the c-a transition is of microwave frequency and the c-b transition is dipole forbidden, the corresponding decay rates γ_μ

and γ_c can be considered small compared to γ. We assume resonance of the driving microwave field, set $r_\mu = r = 0$, and choose $r_c = \gamma$. In this case Eqs. (16) simplify to the expressions

$$\chi' = -\frac{\mathcal{K}^2 N}{\epsilon_0 \hbar} \frac{\Delta}{MDD^*} \left[\frac{3\gamma^3 K_\mu}{4} - \gamma_c(\gamma + K_\mu)\Delta^2 \right] , \tag{20a}$$

$$\chi'' = -\frac{\mathcal{K}^2 N}{\epsilon_0 \hbar} \frac{\gamma^2 K_\mu}{2MDD^*} \left[\frac{\gamma K_\mu}{4} - \Delta^2 + \frac{1}{2}\gamma^2 \right] , \tag{20b}$$

where only the leading terms have been kept, and the denominators DD^* and M read in this simplified version:

$$DD^* = \left[\frac{\gamma K_\mu}{4} - \Delta^2 + \frac{1}{2}\gamma^2 \right]^2 + \frac{9}{4}\gamma^2\Delta^2 , \tag{21}$$

$$M = \gamma^2 + 3\gamma K_\mu . \tag{22}$$

In Fig. 13 the real and imaginary parts of the susceptibility, according to Eqs. (20), are displayed as a function of the detuning Δ. Here we have assumed γ to be purely radiative, i.e., $\gamma = \mathcal{K}^2\nu^3/6\pi\hbar\epsilon_0 c^3$. It immediately becomes obvious from the figure that there is a test-field frequency that experiences both vanishing absorption and a high real part of the susceptibility. The separation of the two absorption peaks increases with increasing Rabi frequency Ω_μ [cf. Eq. (21)]. At the same time, the maximum value of χ' at the point of vanishing absorption decreases.

The decay rates γ_μ and γ_{ca} between the two upper levels strongly increase in the presence of collisions and hence the established coherence is very sensitive to such collisions. The influence of Doppler broadening is displayed in Fig. 14. Since the microwave transition is of much smaller frequency than the optical test-field transition, the effect of Doppler broadening is mainly an averaging of the curve in Fig. 13 over a Gaussian distribution of Δ. The sharp spectral structure is hence quickly washed out if the system becomes inhomogeneously broadened. This effect decreases with increasing Rabi frequency.

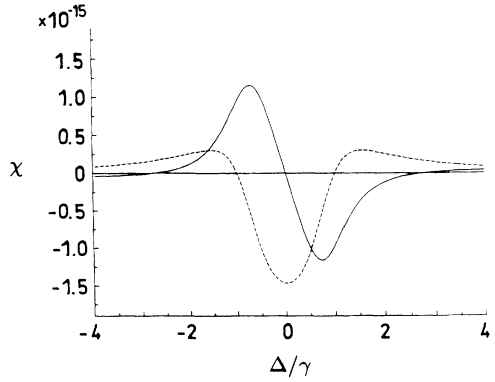

FIG. 13. Real (line) and imaginary (dashed) parts of the linear susceptibility for the upper-level microwave scheme. Here microwave resonance and vanishing r and r_μ are assumed and γ_μ is neglected. We have $\Omega_\mu = r_c = \gamma$ and $\gamma_c = 0.1\gamma$.

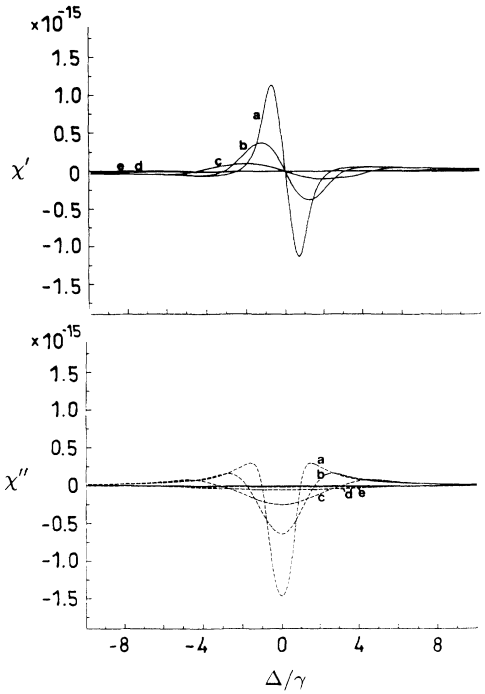

FIG. 14. Influence of Doppler broadening on χ' (upper curves) and χ'' (lower curves) for the upper-level microwave scheme. Here the Dopplerwidth are (a) 0, (b) 1γ, (c) 2γ, (d) 5γ, and (e) 10γ. All other parameters are same as in Fig. 13.

C. Lower-level microwave scheme

The case opposite to the previous one is depicted in Fig. 15, where the lower level of the optical transition under investigation is coupled to a third level c via a strong microwave field. Since some population is necessary in the upper lasing level in order to get a high refractive index with no absorption, we must introduce pump processes. The corresponding equations of motion including the pump and decay processes then read in the appropriate rotating frame:

$$\dot{\rho}_{aa} = -(\gamma + \gamma_c)\rho_{aa} + r\rho_{bb} + r_c\rho_{cc} - i\left[\frac{\mathcal{K}E}{\hbar}\rho_{ba} - \frac{\mathcal{K}E^*}{\hbar}\rho_{ab} \right] , \tag{23a}$$

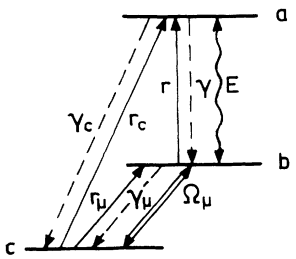

FIG. 15. Level scheme for the lower-level microwave scheme. The transition from a to b is of optical frequency and couples to the test field E. Level b is coupled to a third level c via a strong microwave field of Rabi frequency Ω_μ.

$$\dot{\rho}_{bb}=-(r+\gamma_\mu)\rho_{bb}+\gamma\rho_{aa}+r_\mu\rho_{cc}+i\left[\frac{\wp E}{\hbar}\rho_{ba}-\Omega_\mu\rho_{cb}-\text{c.c.}\right], \tag{23b}$$

$$\dot{\rho}_{cc}=-(r_c+r_\mu)\rho_{cc}+\gamma_c\rho_{aa}+\gamma_\mu\rho_{bb}+i(\Omega_\mu\rho_{cb}-\Omega_\mu^*\rho_{bc}), \tag{23c}$$

$$\dot{\rho}_{ab}=-(i\Delta+\gamma_{ab})\rho_{ab}+i\frac{\wp E}{\hbar}(\rho_{aa}-\rho_{bb})+i\Omega_\mu^*\rho_{ac}, \tag{23d}$$

$$\dot{\rho}_{bc}=-(i\Delta_\mu+\gamma_{bc})\rho_{bc}+i\Omega_\mu(\rho_{bb}-\rho_{cc})-i\frac{\wp E^*}{\hbar}\rho_{ac}, \tag{23e}$$

$$\dot{\rho}_{ac}=-[i(\Delta+\Delta_\mu)+\gamma_{ac}]\rho_{ac}+i\Omega_\mu\rho_{ab}-i\frac{\wp E}{\hbar}\rho_{bc}. \tag{23f}$$

As before, Δ and Δ_μ are the detunings of the test and the microwave fields with respect to the corresponding transitions. Solving for the steady state to first order in the test field E leads to the following general solution for the real and imaginary parts of the polarization:

$$\chi'=-\frac{N\wp^2}{\epsilon_0\hbar DD^*}\frac{1}{M}\left[-(|\Omega_\mu|^2-\Delta^2-\Delta\Delta_\mu+\gamma_{ab}\gamma_{ac})\left\{(\Delta+\Delta_\mu)[(r-\gamma-\gamma_c)(r_c+r_\mu+K_\mu)+r_c(\gamma_\mu+\gamma_c+K_\mu)]-\frac{1}{2}K_\mu\frac{\Delta_\mu}{\gamma_{bc}}[\gamma(r_\mu+r_c-\gamma_\mu)+\gamma_c(r_\mu-\gamma_\mu-r)]\right\}+[\Delta\gamma_{ac}+(\Delta+\Delta_\mu)\gamma_{ab}]\{\gamma_{ac}[(r-\gamma-\gamma_c)(r_c+r_\mu+K_\mu)+r_c(\gamma_\mu+\gamma_c+K_\mu)]+\tfrac{1}{2}K_\mu[\gamma(r_\mu+r_c-\gamma_\mu)+\gamma_c(r_\mu-\gamma_\mu-r)]\}\right], \tag{24a}$$

$$\chi''=-\frac{N\wp^2}{\epsilon_0\hbar DD^*}\frac{1}{M}\left[(|\Omega_\mu|^2-\Delta^2-\Delta\Delta_\mu+\gamma_{ab}\gamma_{ac})\{\gamma_{ac}[(r-\gamma-\gamma_c)(r_c+r_\mu+K_\mu)+r_c(\gamma_\mu+\gamma_c+K_\mu)]+\tfrac{1}{2}K_\mu[\gamma(r_\mu+r_c-\gamma_\mu)+\gamma_c(r_\mu-\gamma_\mu-r)]\}+[\Delta\gamma_{ac}+(\Delta+\Delta_\mu)\gamma_{ab}]\left\{(\Delta+\Delta_\mu)[(r-\gamma-\gamma_c)(r_c+r_\mu+K_\mu)+r_c(\gamma_\mu+\gamma_c+K_\mu)]-\frac{1}{2}K_\mu\frac{\Delta_\mu}{\gamma_{bc}}[\gamma(r_\mu+r_c-\gamma_\mu)+\gamma_c(r_\mu-\gamma_\mu-r)]\right\}\right]. \tag{24b}$$

Here we have used the definitions

$$D=(|\Omega_\mu|^2-\Delta^2-\Delta\Delta_\mu+\gamma_{ab}\gamma_{ac})+i[\Delta\gamma_{ac}+(\Delta+\Delta_\mu)\gamma_{ab}], \tag{25}$$

$$M=(r_c+r_\mu+K_\mu)(r+\gamma_c+\gamma)+(\gamma_\mu+K_\mu)(r_c+\gamma_c+\gamma)+\gamma_c(r-r_c), \tag{26}$$

$$K_\mu=\frac{2\gamma_{bc}|\Omega_\mu|^2}{\Delta_\mu^2+\gamma_{bc}^2}. \tag{27}$$

As before, we proceed by restricting this result to the case of microwave resonance $\Delta_\mu=0$ and no pumping on the allowed optical transition, i.e., $r=r_\mu=0$. Furthermore, we neglect the microwave decay γ_μ and the decay γ_c of the dipole-forbidden transition a-c, and choose $r_c=\gamma$. In this case,

$$\chi'=-\frac{\wp^2N}{\epsilon_0\hbar}\frac{\Delta\gamma^2}{MDD^*}\left[\frac{\gamma K_\mu}{4}-\Delta^2+\frac{1}{2}\gamma^2+\frac{3}{2}\gamma\left[\frac{1}{2}K_\mu-\gamma\right]\right], \tag{28a}$$

$$\chi''=-\frac{\wp^2N}{\epsilon_0\hbar}\frac{\gamma^2}{MDD^*}\left[\left[\frac{\gamma K_\mu}{4}-\Delta^2+\frac{1}{2}\gamma^2\right]\left[\frac{1}{2}K_\mu-\gamma\right]-\frac{3}{2}\gamma\Delta^2\right], \tag{28b}$$

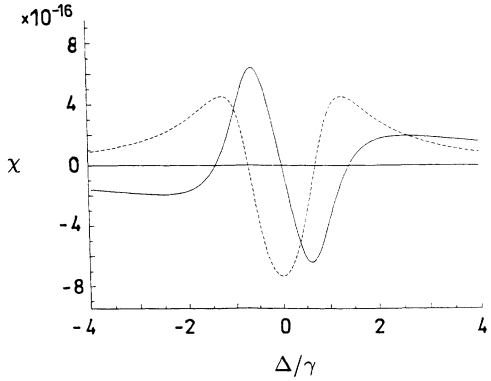

FIG. 16. Real (line) and imaginary (dashed) parts of the linear susceptibility for the lower-level microwave scheme. Here microwave resonance and vanishing r and r_μ are assumed and γ_μ and γ_c are neglected. We have $\Omega_\mu=r_c=\gamma$.

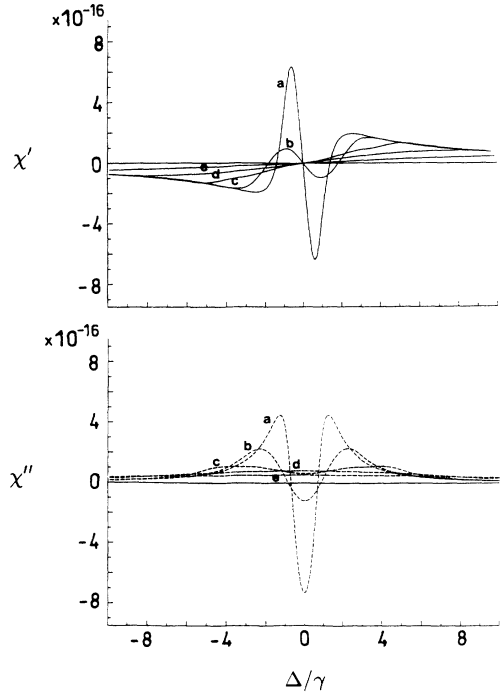

FIG. 17. Influence of Doppler broadening on χ' (upper curves) and χ'' (lower curves) in the lower-level microwave scheme. The Dopplerwidth are (a) 0, (b) 1γ, (c) 2γ, (d) 5γ, and (e) 10γ. All other parameters are same as in Fig. 16.

where DD^* and M again take the simple form given in Eqs. (21) and (22). In Fig. 16, χ' and χ'' are depicted for this special case. Again, there is a point with no absorption or emission, but with a large value of the real part of the susceptibility. According to Eqs. (24), (25), the separation of the two absorption maxima increases with growing microwave field strength.

In the case discussed here, the coherence between b and c is less sensitive to collisions, since the corresponding wave functions are located close to the atomic nucleus. However, Doppler broadening strongly diminishes the maximum value of χ' at the point of vanishing absorption, as visible from Fig. 17, for the same reason as mentioned in Sec. III B. Here again Doppler broadening becomes less important if the Rabi frequency of the driving microwave field increases.

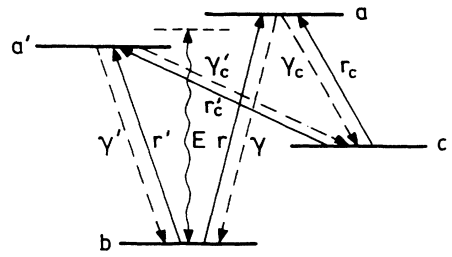

FIG. 18. The radiative decay of two closely spaced upper levels a and a' of the same J and m_J quantum numbers to common levels b and c generates quantum interference and coherence between the two upper levels.

IV. HIGH INDEX OF REFRACTION PRODUCED BY INCOHERENT PROCESSES

In this section we show that atomic coherence or interference of pathways can be established even by incoherent processes. For example, the radiative decay of two closely spaced levels a and a' to common levels may lead to atomic coherence if the selection rules are such that the corresponding transitions from a and a' couple to the same vacuum modes with the same strength [3]. In order to realize this interference effect there must be the restrictive requirement that two closely spaced levels have the same J and m_J quantum numbers. In analogy to the coupling of spontaneous emission, the interference of incoherent pump processes can lead to atomic coherence as well [10]. In this section we demonstrate that coherent processes like these can produce media with high dispersion without absorption or gain. We restrict ourselves to presenting and discussing the main results.

A. Interference of radiative decay processes

Let us consider the level configuration sketched in Fig. 18. Two closely lying levels a and a' decay radiatively to two lower levels b and c. We assume that the quantum numbers of both levels are such that the transitions from a and a' interact with the same vacuum modes. Including (indirect) pump mechanisms, the equations of motion of the density matrix read in a rotating frame:

$$\dot{\rho}_{aa}=-(\gamma+\gamma_c)\rho_{aa}-\tfrac{1}{2}[(\gamma\gamma')^{1/2}+(\gamma_c\gamma_c')^{1/2}](\rho_{aa'}+\rho_{a'a})+r\rho_{bb}+r_c\rho_{cc}-i\frac{\wp}{\hbar}(E\rho_{ba}-\text{c.c.})\,, \tag{29a}$$

$$\dot{\rho}_{a'a'}=-(\gamma'+\gamma_c')\rho_{a'a'}-\tfrac{1}{2}[(\gamma\gamma')^{1/2}+(\gamma_c\gamma_c')^{1/2}](\rho_{aa'}+\rho_{a'a})+r'\rho_{bb}+r_c'\rho_{cc}-i\frac{\wp'}{\hbar}(E\rho_{ba'}-\text{c.c.})\,, \tag{29b}$$

$$\dot{\rho}_{bb}=-(r+r')\rho_{bb}+(\gamma\gamma')^{1/2}(\rho_{aa'}+\rho_{a'a})+\gamma\rho_{aa}+\gamma'\rho_{a'a'}+i\frac{\wp}{\hbar}(E\rho_{ba}-\text{c.c.})+i\frac{\wp'}{\hbar}(E\rho_{ba'}-\text{c.c.})\,, \tag{29c}$$

$$\dot{\rho}_{aa'}=-[i\omega_{aa'}+\tfrac{1}{2}(\gamma+\gamma'+\gamma_c+\gamma_c')]\rho_{aa'}-\tfrac{1}{2}[(\gamma\gamma')^{1/2}+(\gamma_c\gamma_c')^{1/2}](\rho_{aa}+\rho_{a'a'})-i\frac{\wp}{\hbar}E\rho_{ba'}+i\frac{\wp'}{\hbar}E^*\rho_{ab}\,, \tag{29d}$$

$$\dot{\rho}_{ab}=-[i\Delta_{ab}+\tfrac{1}{2}(\gamma+r+r'+\gamma_c)]\rho_{ab}-\tfrac{1}{2}[(\gamma\gamma')^{1/2}+(\gamma_c\gamma_c')^{1/2}]\rho_{a'b}-i\frac{\wp E}{\hbar}(\rho_{bb}-\rho_{aa})+i\frac{\wp' E}{\hbar}\rho_{aa'}\,, \tag{29e}$$

$$\dot{\rho}_{a'b}=-[i\Delta_{a'b}+\tfrac{1}{2}(\gamma'+r+r'+\gamma_c')]\rho_{a'b}-\tfrac{1}{2}[(\gamma\gamma')^{1/2}+(\gamma_c\gamma_c')^{1/2}]\rho_{ab}-i\frac{\wp' E}{\hbar}(\rho_{bb}-\rho_{a'a'})+i\frac{\wp E}{\hbar}\rho_{a'a}\,. \tag{29f}$$

As before, Δ_{ab} and $\Delta_{a'b}$ are the detunings of the test field E with respect to the two optical transitions, and we have introduced pump processes in order to maintain some upper-level population. Here we especially call attention to the $(\gamma\gamma')^{1/2}$ terms, which are due to the quantum interference of the decay processes. A derivation of these terms is given in Refs. [3] and [13]. Solving for steady state to first order in the test field, we obtain the following general expressions for the real and imaginary parts of the susceptibility:

$$\chi' = \frac{\wp^2 N}{\epsilon_0 \hbar D^* D} \left\{ \left[\frac{\Delta}{2}[(1+\kappa^2)(\gamma+\gamma_c)+4r] - \frac{\omega}{4}(1-\kappa^2)(\gamma+\gamma_c) \right] \right.$$
$$\times \left[\gamma(1+\kappa^2) \left[1 - \frac{(1+\kappa^2)(\gamma+\gamma_c)\gamma_{aa'}}{2(\omega_{aa'}^2+\gamma_{aa'}^2)} \right] - 2r + \frac{(1+\kappa^2)(\gamma+\gamma_c)\gamma_{aa'} r}{(\omega_{aa'}^2+\gamma_{aa'}^2)} - \frac{(1+\kappa^2)(\gamma+\gamma_c)\omega_{aa'}^2}{2(\omega_{aa'}^2+\gamma_{aa'}^2)} \right]$$
$$+ \left[\frac{\omega_{aa'}^2}{4} - \Delta^2 + r^2 + \frac{r}{2}(1+\kappa^2)(\gamma+\gamma_c) \right]$$
$$\times \left[\frac{\omega}{2}(1-\kappa^2)\frac{\gamma}{r} \left[1 - \frac{(1+\kappa^2)(\gamma+\gamma_c)\gamma_{aa'}}{2(\omega_{aa'}^2+\gamma_{aa'}^2)} \right] + 2\Delta \right.$$
$$\left. \left. - \Delta(1+\kappa^2)\frac{\gamma}{r} \left[1 - \frac{(1+\kappa^2)(\gamma+\gamma_c)\gamma_{aa'}}{2(\omega_{aa'}^2+\gamma_{aa'}^2)} \right] - \Delta \frac{(1+\kappa^2)(\gamma+\gamma_c)\gamma_{aa'}}{(\omega_{aa'}^2+\gamma_{aa'}^2)} \right] \right\} \rho_{aa}^{(0)} \tag{30a}$$

$$\chi'' = -\frac{\wp^2 N}{\epsilon_0 \hbar D^* D} \left\{ \left[\frac{\Delta}{2}[(1+\kappa^2)(\gamma+\gamma_c)+4r] - \frac{\omega}{4}(1-\kappa^2)(\gamma+\gamma_c) \right] \right.$$
$$\times \left[\frac{\omega}{2}(1-\kappa^2)\frac{\gamma}{r} \left[1 - \frac{(1+\kappa^2)(\gamma+\gamma_c)\gamma_{aa'}}{2(\omega_{aa'}^2+\gamma_{aa'}^2)} \right] + 2\Delta \right.$$
$$\left. - \Delta(1+\kappa^2)\frac{\gamma}{r} \left[1 - \frac{(1+\kappa^2)(\gamma+\gamma_c)\gamma_{aa'}}{2(\omega_{aa'}^2+\gamma_{aa'}^2)} \right] - \Delta \frac{(1+\kappa^2)(\gamma+\gamma_c)\gamma_{aa'}}{(\omega_{aa'}^2+\gamma_{aa'}^2)} \right]$$
$$- \left[\frac{\omega_{aa'}^2}{4} - \Delta^2 + r^2 + \frac{r}{2}(1+\kappa^2)(\gamma+\gamma_c) \right]$$
$$\times \left[\gamma(1+\kappa^2) \left[1 - \frac{(1+\kappa^2)(\gamma+\gamma_c)\gamma_{aa'}}{2(\omega_{aa'}^2+\gamma_{aa'}^2)} \right] - 2r \right.$$
$$\left. \left. + \frac{(1+\kappa^2)(\gamma+\gamma_c)\gamma_{aa'} r}{(\omega_{aa'}^2+\gamma_{aa'}^2)} - \frac{(1+\kappa^2)(\gamma+\gamma_c)\omega_{aa'}^2}{2(\omega_{aa'}^2+\gamma_{aa'}^2)} \right] \right\} \rho_{aa}^{(0)} \tag{30b}$$

The denominator term D^*D takes the form

$$D^*D = \left[\frac{\omega_{aa'}^2}{4} - \Delta^2 + r^2 + \frac{r}{2}(\gamma+\gamma_c)(1+\kappa^2) \right]^2$$
$$+ \left[\frac{\Delta}{2}[4r + (1+\kappa^2)(\gamma+\gamma_c)] \right.$$
$$\left. - \frac{\omega_{aa'}}{4}(1-\kappa^2)(\gamma+\gamma_c) \right]^2 , \tag{31a}$$

and

$$\rho_{aa}^{(0)} = \left[1 + \frac{1}{\kappa^2} + \left[\frac{\gamma}{r} + \frac{\gamma_c}{r_c} \right] \right.$$
$$\left. \times \left[1 - \frac{(\gamma+\gamma_c)\gamma_{aa'}(1+\kappa^2)}{2(\omega_{aa'}^2+\gamma_{aa'}^2)} \right] \right]^{-1} , \tag{31b}$$

with $\kappa = \wp'/\wp = \wp_c'/\wp_c$ and $r' = r, r_c' = r_c$. The parameters $\wp$ and $\wp'$ are the dipole matrix elements for the a-b and a'-b transitions and $\wp_c$ and $\wp_c'$ are the corresponding dipole matrix elements for the transitions to c. To better illustrate the physical processes described by these complex formulas, we assume $r = \gamma/2$, $r_c = \gamma_c/2$, and $\kappa = 1$. Then Eqs. (30) simplify to

$$\chi' = -\frac{\wp^2 N \Delta}{\epsilon_0 \hbar D^* D} \left[(3\gamma+\gamma_c)\gamma_c + \frac{\omega_{aa'}^2}{2} - 2\Delta^2 + \frac{3}{2}\gamma^2 \right]$$
$$\times \frac{\omega_{aa'}^2}{\omega_{aa'}^2 + (\gamma+\gamma_c)^2} \rho_{aa}^{(0)} , \tag{32a}$$

$$\chi'' = \frac{\wp^2 N}{\epsilon_0 \hbar D^* D} \left[2\Delta^2(2\gamma+2\gamma_c) \right.$$
$$\left. - \left[\frac{\omega_{aa'}^2}{4} + \frac{3}{4}\gamma^2 + \frac{\gamma\gamma_c}{2} \right] \gamma_c \right]$$
$$\times \frac{\omega_{aa'}^2}{\omega_{aa'}^2 + (\gamma+\gamma_c)^2} \rho_{aa}^{(0)} , \tag{32b}$$

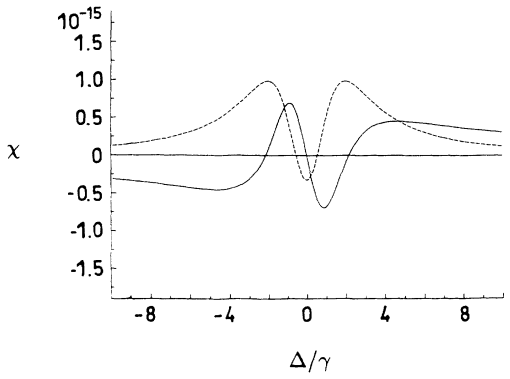

FIG. 19. Real (line) and imaginary (dashed) parts of the linear susceptibility for the case of interfering radiative decays. $\omega_{aa'}=2\gamma$, $r_c=r=\gamma$.

with

$$D^*D=\left[\frac{\omega_{aa'}^2}{4}-\Delta^2+2\gamma^2+\gamma\gamma_c\right]^2+\Delta^2(3\gamma+\gamma_c)^2$$

and

$$\rho_{aa}^{(0)}=\left[6-\frac{4(\gamma+\gamma_c)^2}{\omega_{aa'}^2+(\gamma+\gamma_c)^2}\right]^{-1}.$$

Figure 19 displays the real and imaginary parts of the susceptibility as functions of the detuning $\Delta=(\Delta_{ab}+\Delta_{a'b})/2$. Again, frequencies of perfect transparency and a high index of refraction exist.

Interference of radiative decays occurs only if the transitions from a and a' share the same vacuum modes. Hence, the spacing between the two levels is limited to approximately 2γ, and therefore the spectral shape of $\chi'(\Delta)$ and $\chi''(\Delta)$ is narrow. As a consequence, already a small Doppler broadening washes out the characteristic behavior of the curves, as demonstrated in Fig. 20.

B. Interference of incoherent pump processes—upper-level doublet

An essential disadvantage of the previous scheme is that its practical implementation requires an atomic system with two levels spaced so closely that they are within twice the natural linewidth, and which also have the same J and m_J quantum numbers. An effect similar to the interference of radiative decay processes can be achieved, however, by interference of incoherent pump processes, which does not imply such restrictive conditions [10].

In the case of interfering radiative decays, both affected transitions need to couple in the same way to the same vacuum modes, which have arbitrary polarizations. Hence, the two upper levels must have the same J and m_J quantum numbers. In the scheme discussed here, which makes use of linearly polarized pump light, the interference can be produced even between magnetic sublevels. Moreover, in contrast to the previous case, the level spacing need only be smaller than the spectral width of the pump field.

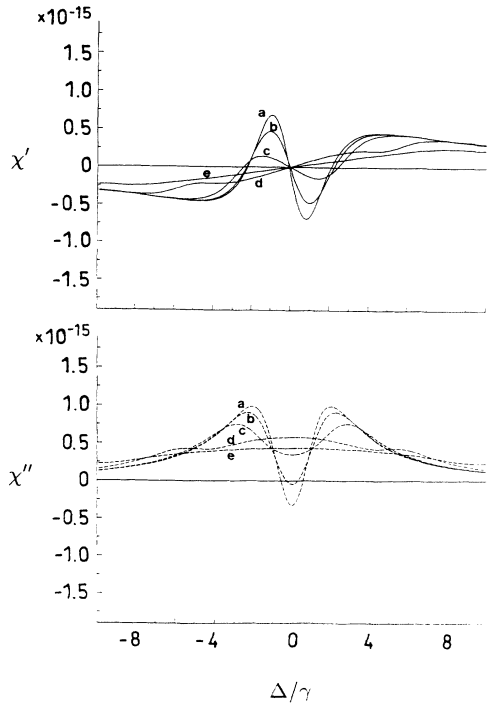

FIG. 20. Influence of Doppler broadening on χ' (upper curves) and χ'' (lower curves) for the case of interference of radiative decays. The corresponding width is (a) 0, (b) 1γ, (c) 2γ, (d) 5γ, and (e) 10γ. All other parameters are same as in Fig. 19. Because of the narrow spectral structure of $\chi(\Delta)$, already a small inhomogeneous broadening washes out the coherence effect.

Let us consider the level scheme sketched in Fig. 21. An upper-level doublet a and a' is pumped to a level c simultaneously by an incoherent field. When the decay and pump processes are included, the equations of motion for the density-matrix elements in an appropriate rotating frame are

$$\dot{\rho}_{cc}=-(r_c+r_c'+\gamma_c+\gamma_c'+\gamma_b)\rho_{cc}+r_c\rho_{aa}+r_c'\rho_{a'a'}+(r_cr_c')^{1/2}(\rho_{a'a}+\rho_{aa'}), \tag{33a}$$

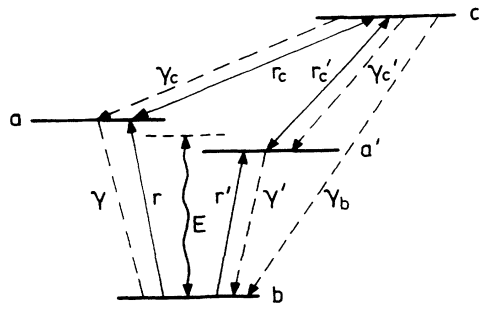

FIG. 21. Interference effects between two upper levels a and a' occur if both levels are driven to a level c with a strong incoherent pump field.

$$\dot{\rho}_{aa}=-(\gamma+r_c)\rho_{aa}+r\rho_{bb}+(r_c+\gamma_c)\rho_{cc} -\tfrac{1}{2}(r_c r_c')^{1/2}(\rho_{a'a}+\rho_{aa'})-i\left[\frac{\wp E}{\hbar}\rho_{ba}-\text{c.c.}\right], \quad (33b)$$

$$\dot{\rho}_{a'a'}=-(\gamma'+r_c')\rho_{a'a'}+r'\rho_{bb}+(r_c'+\gamma_c')\rho_{cc} -\tfrac{1}{2}(r_c r_c')^{1/2}(\rho_{a'a}+\rho_{aa'})-i\left[\frac{\wp' E}{\hbar}\rho_{ba'}-\text{c.c.}\right], \quad (33c)$$

$$\dot{\rho}_{bb}=-(r+r')\rho_{bb}+\gamma\rho_{aa}+\gamma'\rho_{a'a'}+\gamma_b\rho_{cc} +i\left[\frac{\wp E}{\hbar}\rho_{ba}+\frac{\wp' E}{\hbar}\rho_{ba'}-\text{c.c.}\right], \quad (33d)$$

$$\dot{\rho}_{aa'}=-\left[i\omega_{aa'}+\frac{1}{2}(r_c+r_c'+\gamma+\gamma')\right]\rho_{aa'} -\tfrac{1}{2}(r_c r_c')^{1/2}(\rho_{aa}+\rho_{a'a'}-2\rho_{cc}) +i\frac{\wp' E^*}{\hbar}\rho_{ab}-i\frac{\wp E}{\hbar}\rho_{ba'}, \quad (33e)$$

$$\dot{\rho}_{ab}=-\left[i\Delta_{ab}+\frac{1}{2}(r+r'+\gamma+r_c)\right]\rho_{ab} -\tfrac{1}{2}(r_c r_c')^{1/2}\rho_{a'b}-i\frac{\wp E}{\hbar}(\rho_{bb}-\rho_{aa})+i\frac{\wp' E}{\hbar}\rho_{aa'}, \quad (33f)$$

$$\dot{\rho}_{a'b}=-\left[i\Delta_{a'b}+\frac{1}{2}(r'+r+\gamma'+r_c')\right]\rho_{a'b} -\tfrac{1}{2}(r_c r_c')^{1/2}\rho_{ab}-i\frac{\wp' E}{\hbar}(\rho_{bb}-\rho_{a'a'})+i\frac{\wp E}{\hbar}\rho_{a'a}. \quad (33g)$$

Here we have introduced the detunings Δ_{ab} and $\Delta_{a'b}$ of the test-field frequency with respect to the two transitions under investigation. The $(r_c r_c')^{1/2}$ terms in Eqs. (33) are similar to the $(\gamma\gamma')^{1/2}$ terms in the case of interfering radiative decays and originate from the interference of the pump processes. A derivation of these terms is given in Ref. [10]. As can be seen from Eq. (33c), the upper-level coherence is proportional to the sum of the upper-level population minus twice the population in the auxiliary level c. In order to have large coherence, the decay rate from level c should be large. Hence we assume a large decay rate from level c to the lower level, $\gamma_b\to\infty$. Further making the reasonable simplifying assumptions $\wp=\wp'$, $\gamma_c=\gamma_c'$, $r'=r$, and $r_c'=r_c$, we obtain for the real and imaginary parts of the polarization

$$\chi'=\frac{\wp^2 N\rho_{aa}^{(0)}\Delta}{\epsilon_0\hbar MD^*D}\left[2\left[r^2+r\gamma+\frac{1}{4}(\gamma^2-\omega_{aa'}^2)+\Delta^2\right]\left[\frac{r_c+\gamma}{r}(\omega_{aa'}^2+\gamma^2+2\gamma r_c+rr_c)-[\omega_{aa'}^2+(\gamma+r_c)^2]\right] -\omega_{aa'}^2 r_c(2r+\gamma+r_c)\right], \quad (34a)$$

$$\chi''=\frac{\wp^2 N\rho_{aa}^{(0)}}{\epsilon_0\hbar MD^*D}\left\{\left[(2r+\gamma)\left[r^2+\frac{1}{4}\gamma^2+\frac{1}{2}\gamma r_c+r(\gamma+r_c)-\Delta^2+\frac{1}{4}\omega_{aa'}^2\right]+2\Delta^2(2r+\gamma+r_c)\right] \times\left[\frac{r_c+\gamma}{r}(\omega_{aa'}^2+\gamma^2+2\gamma r_c+rr_c)-[\omega_{aa'}^2+(\gamma+r_c)^2]\right] -\omega_{aa'}^2 r_c\left[r^2+\frac{1}{4}\gamma^2+\frac{1}{2}\gamma r_c+r(\gamma+r_c)-\Delta^2+\frac{1}{4}\omega_{aa'}^2\right]\right\}, \quad (34b)$$

where we have used the definitions

$$D^*D=[r^2+\tfrac{1}{4}\gamma^2+\tfrac{1}{2}\gamma r_c+r(\gamma+r_c)-\Delta^2+\tfrac{1}{4}\omega_{aa'}^2]^2 +\Delta^2(2r+\gamma+r_c)^2, \quad M=\omega_{aa'}^2+(\gamma+r_c)^2, \quad (35)$$

and $\Delta=(\Delta_{ab}+\Delta_{a'b})/2$. For the case discussed here, the zeroth-order population in the two upper levels a and a' are equal and have the value

$$\rho_{aa}^{(0)}=\left[\frac{r_c+\gamma}{r}\left[1-\frac{r_c^2}{(\gamma+r_c)^2+\omega_{aa'}^2}\right]+2\right]^{-1}. \quad (36)$$

In Fig. 22 the real and imaginary parts of the susceptibility are displayed as a function of the test-field detuning Δ. Obviously, the coherence between the upper levels

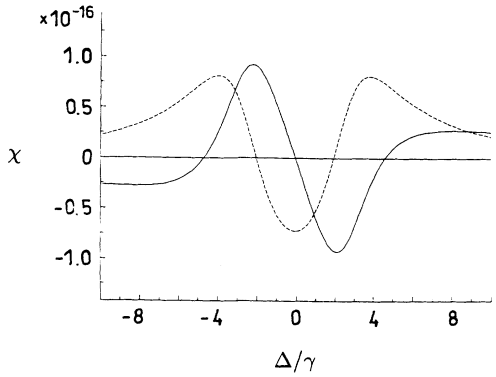

FIG. 22. Real (line) and imaginary (dashed) parts of the linear susceptibility for the case of interference via incoherent pump processes (upper-level scheme). The corresponding parameter values are $\omega_{aa'}=5\gamma, r_c=0.5\gamma, r=1.45\gamma$.

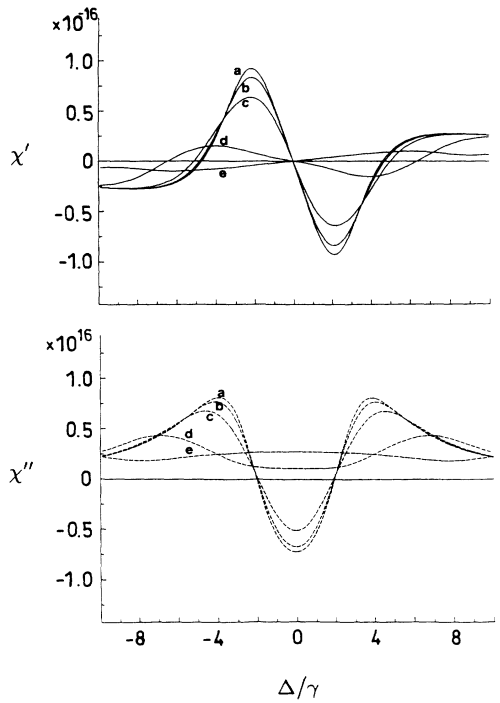

FIG. 23. Influence of Doppler broadening on χ' (upper curves) and χ'' (lower curves) for the case of interference of pump processes. The corresponding width is (a) 0, (b) 1γ, (c) 2γ, (d) 5γ, and (e) 10γ. All other parameters are same as in Fig. 22.

generated by the interference of the two pump processes can lead to frequency values for which the imaginary part vanishes, while the real part of the susceptibility still has a substantial value.

Since the coherence here is established between upper levels, the refractive index at a point of vanishing absorption is sensitive to collisions. Moreover, Doppler broadening affects only the optical transition, since the pump-field spectrum is assumed broad. As a consequence, Doppler broadening averages the spectral structure displayed in Fig. 22 and rapidly diminishes the achievable value of χ' (see Fig. 23).

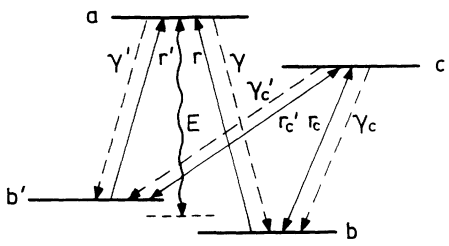

FIG. 24. In contrast to the case discussed in Sec. IV A, incoherent pump processes can cause interferences and hence may create coherence between a lower-level doublet b and b'.

C. Interference of incoherent pump processes—lower-level doublet

In contrast to the interference due to radiative decays, the pump processes can be used to create lower-level coherence. We now investigate such a situation.

We consider here an ensemble of atoms with the level configuration sketched in Fig. 24. Two closely lying lower levels b and b', with magnetic quantum numbers $m=1$ and -1, are pumped by a linearly polarized incoherent field to a level c with $m=0$. Both transitions interact with the same pump mode, establishing coherence between b and b'. Including the (indirect) pump processes to the upper lasing level a and the decay processes as indicated in Fig. 24, we obtain the equations of motion of the density matrix in an appropriate rotating frame:

$$\dot{\rho}_{cc}=-(r_c+r_c'+\gamma_c+\gamma_c')\rho_{cc}+r_c\rho_{bb}+r_c'\rho_{b'b'}+(r_cr_c')^{1/2}(\rho_{b'b}+\rho_{bb'}) , \tag{37a}$$

$$\dot{\rho}_{aa}=-(\gamma+\gamma')\rho_{aa}+r\rho_{bb}+r'\rho_{b'b'}+i\left[\frac{\not{\wp}E^*}{\hbar}\rho_{ab}+\frac{\not{\wp}'E^*}{\hbar}\rho_{ab'}-\text{c.c.}\right] , \tag{37b}$$

$$\dot{\rho}_{bb}=-(r+r_c)\rho_{bb}+\gamma\rho_{aa}+r_c\rho_{cc}-\frac{1}{2}(r_cr_c')^{1/2}(\rho_{b'b}+\rho_{bb'})-i\left[\frac{\not{\wp}E^*}{\hbar}\rho_{ab}-\text{c.c.}\right] , \tag{37c}$$

$$\dot{\rho}_{b'b'}=-(r'+r_c')\rho_{b'b'}+\gamma'\rho_{aa}+r_c'\rho_{cc}-\frac{1}{2}(r_cr_c')^{1/2}(\rho_{b'b}+\rho_{bb'})-i\left[\frac{\not{\wp}'E^*}{\hbar}\rho_{ab'}-\text{c.c.}\right] , \tag{37d}$$

$$\dot{\rho}_{bb'}=-\left[i\omega_{bb'}+\frac{1}{2}(r+r'+r_c+r_c')\right]\rho_{bb'}-\frac{1}{2}(r_cr_c')^{1/2}(\rho_{bb}+\rho_{b'b'}-2\rho_{cc})-i\left[\frac{\not{\wp}E^*}{\hbar}\rho_{ab'}-\frac{\not{\wp}'E}{\hbar}\rho_{ba}\right] , \tag{37e}$$

$$\dot{\rho}_{ab}=-\left[i\Delta_{ab}+\frac{1}{2}(r+r_c+\gamma+\gamma')\right]\rho_{ab}-\frac{1}{2}(r_cr_c')^{1/2}\rho_{ab'}-i\frac{\not{\wp}E}{\hbar}(\rho_{bb}-\rho_{aa})-i\frac{\not{\wp}'E}{\hbar}\rho_{b'b} , \tag{37f}$$

$$\dot{\rho}_{ab'}=-\left[i\Delta_{ab'}+\frac{1}{2}(r'+r_c'+\gamma+\gamma')\right]\rho_{ab'}-\frac{1}{2}(r_cr_c')^{1/2}\rho_{ab}-i\frac{\not{\wp}'E}{\hbar}(\rho_{b'b'}-\rho_{aa})-i\frac{\not{\wp}E}{\hbar}\rho_{bb'} . \tag{37g}$$

Δ_{ab} and $\Delta_{ab'}$ are the detunings of the test field E with respect to the dipole-allowed transitions a-b and a-b'. Making the reasonable assumptions that $\not{\wp}=\not{\wp}'$, $r_c'=r_c$, $\gamma=\gamma'$, $\gamma_c=\gamma_c'$, and $r'=r$, we obtain for the real and imaginary parts of the susceptibility

$$\chi'=\frac{\mathcal{N}^2 N\rho_{bb}^{(0)}\Delta}{\epsilon_0\hbar MD^*D}\left\{2\left[\gamma^2+r\gamma+\frac{1}{4}(r^2-\omega_{b'b}^2)+\Delta^2\right]\left[\left[1-\frac{r}{\gamma}\right]\{(r_c+\gamma_c)[\omega_{b'b}^2+(r+r_c)^2]-r_c^2(r+r_c)\}\right.\right.$$
$$\left.\left.-r_c\gamma_c(r+r_c)\right]-\omega_{b'b}^2 r_c\gamma_c(2\gamma+r+r_c)\right\}, \tag{38a}$$

$$\chi''=\frac{\mathcal{N}^2 N\rho_{bb}^{(0)}}{\epsilon_0\hbar MD^*D}\left\{\left[(2\gamma+r)\left[\gamma^2+\frac{1}{4}r^2+\frac{1}{2}rr_c+\gamma(r+r_c)-\Delta^2+\frac{1}{4}\omega_{b'b}^2\right]+2\Delta^2(2\gamma+r+r_c)\right]\right.$$
$$\times\left[\left[1-\frac{r}{\gamma}\right]\{(r_c+\gamma_c)[\omega_{b'b}^2+(r+r_c)^2]-\gamma_c^2(r+r_c)\}-r_c\gamma_c(r+r_c)\right]$$
$$\left.-\omega_{b'b}^2 r_c\gamma_c\left[\gamma^2+\frac{1}{4}r^2+\frac{1}{2}rr_c+\gamma(r+r_c)-\Delta^2+\frac{1}{4}\omega_{b'b}^2\right]\right\}, \tag{38b}$$

where we have used the definitions

$$D^*D=[\gamma^2+\tfrac{1}{4}r^2+\tfrac{1}{2}rr_c+\gamma(r+r_c)-\Delta^2+\tfrac{1}{4}\omega_{b'b}^2]^2+\Delta^2(2\gamma+r+r_c)^2,$$
$$M=[\omega_{b'b}^2+(r+r_c)^2](r_c+\gamma_c)-r_c^2(r+r_c), \tag{39}$$

and have introduced the detuning $\Delta=(\Delta_{ab}+\Delta_{ab'})/2$ of the test field with respect to the midfrequency of the two transitions under investigation. The zeroth-order population $\rho_{bb}^{(0)}=\rho_{b'b'}^{(0)}$ of the lower levels is then

$$\rho_{bb}^{(0)}=\left[2+\frac{r}{\gamma}+\frac{r_c[(r_c+r)^2+\omega_{b'b}^2-r_c(r+r_c)]}{(r_c+\gamma_c)[(r_c+r)^2+\omega_{b'b}^2]-r_c^2(r+r_c)}\right]^{-1}. \tag{40}$$

In Fig. 25 we display the real and imaginary parts of the polarization as a function of Δ. Note that again some pumping to the upper level a is necessary in order to have a high refractive index and vanishing absorption. The occurrence of frequency values with vanishing absorption and high refractive index is evident.

The lower-level doublet structure considered here is, of course, more robust against collisional broadening. However, because of the same reasons as in the previous case, the system is again sensitive to Doppler broadening, as displayed in Fig. 26.

V. PRACTICAL IMPLEMENTATION OF INDEX ENHANCEMENT

In this section we want to propose some real atomic systems in which quantum coherence and interference may lead to an ultra-high index of refraction at a point of zero absorption. A favorable atom for a practical realization of the Raman scheme is samarium, whose level scheme is indicated in Fig. 27. Because of its zero nu-

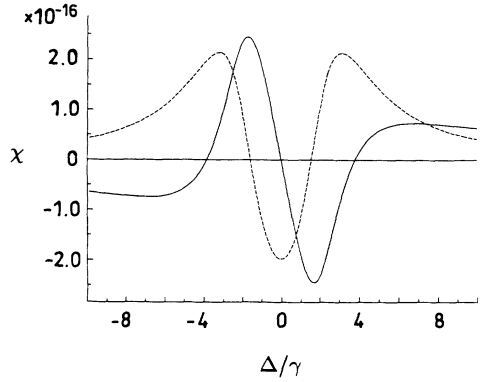

FIG. 25. Real (line) and imaginary (dashed) parts of the linear susceptibility for the case of interference via incoherent pump processes (lower-level scheme). The corresponding parameter values are $\omega_{aa'}=5\gamma$, $r_c=0.5\gamma$, $r=1.45\gamma$.

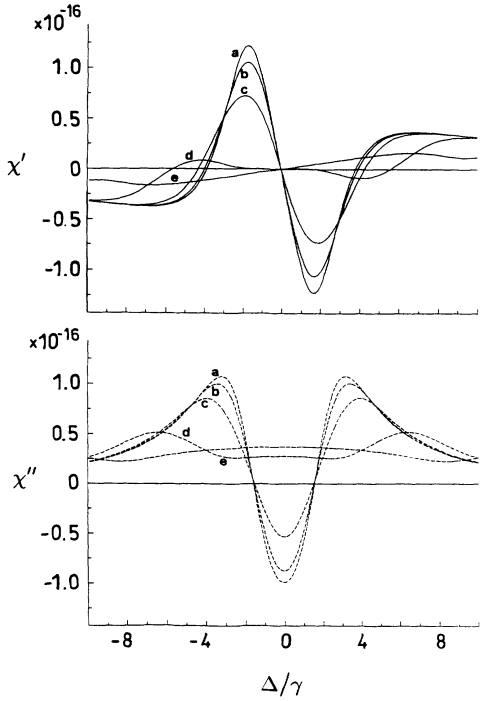

FIG. 26. Influence of Doppler broadening on χ' (upper curves) and χ'' (lower curves) for the case of interference of pump processes. The corresponding width is (a) 0, (b) 1γ, (c) 2γ, (d) 5γ, and (e) 10γ. All other parameters are same as in Fig. 25.

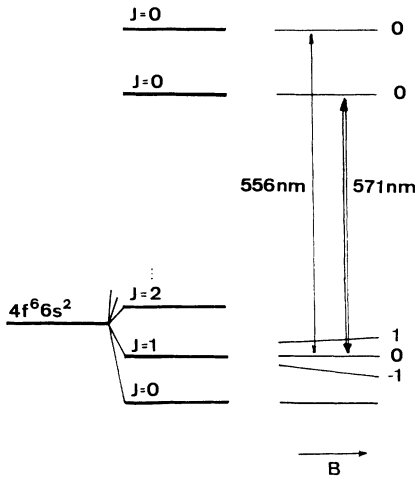

FIG. 27. Atomic-level scheme of samarium.

clear spin, there is no hyperfine splitting and the $m_J = \pm 1$ magnetic sublevels of the $J=1$ manifold of the even ground state may serve as lower levels of the Raman scheme. An applied magnetic field yields the required level splitting. A strong driving field indicated in Fig. 27 by the double line propagating almost parallel to the magnetic field creates atomic coherence between the two sublevels. To avoid a strong optical pumping into the $m_J=0$ ground state by the driving field, it should have a small field component parallel to the magnetic field. This can be realized by providing a small angle between the propagation direction of the field and the magnetic field. An additional pump process from the $m_J=0$ ground state to the upper level of the 556-nm test-field transition then leads to an ultrahigh index of refraction at a point of zero absorption.

Other favorable atomic schemes are alkaline atoms like sodium or rubidium. In Fig. 28, a possible realization of (a) the upper-level microwave scheme and (b) the Raman scheme in rubidium are indicated. The driving fields are

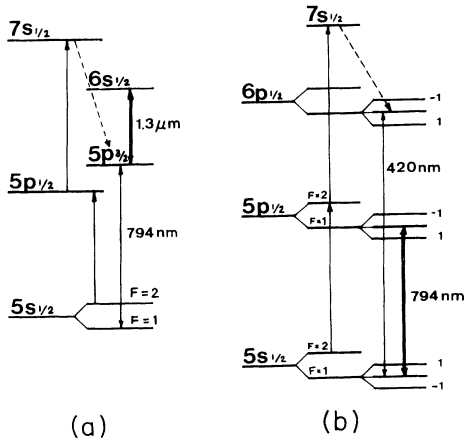

FIG. 28. Atomic-level scheme of rubidium. Realizations of (a) the upper-level microwave and (b) the Raman scheme are indicated.

indicated by double lines and an index enhancement is established on the 794-nm test-field transition. The necessary pump processes are indicated too.

VI. INDEX ENHANCEMENT VIA A MIXTURE OF DIFFERENT TWO-LEVEL ATOMS VERSUS INDEX ENHANCEMENT IN COHERENT ATOMS

We have shown that atomic coherence in multilevel atomic systems can lead to a transparent medium with an ultralarge index of refraction. Perhaps a simpler way to achieve a high index of refraction without using atomic coherence is an incoherent superposition of two-level atoms with slightly different transition frequencies. An example for such a system is depicted in Fig. 29. One kind of atom with the transition frequency ω_1 is in its ground state and another kind of atom with a slightly different transition frequency ω_2 is in its excited state due to some pumping mechanism. For some frequency $\nu, \omega_1 < \nu < \omega_2$, a probe field can experience zero absorption and a high index of refraction.

The calculation of the (exact) susceptibility for this scheme is given in Appendix A. The two two-level model obviously has the advantage of not requiring atomic coherence, which might be difficult to achieve for some of the schemes discussed. On the other hand, this model has some essential disadvantages compared to the coherent schemes, which would seem to make its practical implementation very difficult. Here we give a brief discussion of some of the problems associated with the two two-level model.

In the two two-level model the absorption (χ'') is proportional to $AN_1 - BN_2$, where A and B are some (positive) coefficients given in Eq. (A2b) and N_1 and N_2 are the number densities of the two atomic species. For $AN_1 = BN_2$, we have zero absorption. However, spatial fluctuations in N_1 or N_2 will lead to fluctuations in χ''. That is to say, the field in some regions will experience amplification, while in other regions it will be absorbed. Consequently, the field will develop large spatial intensity fluctuations.

In order to avoid these fluctuations, the two kind of atoms need to be mixed evenly and we cannot use atomic beams. For atomic cells, however, the Doppler effect must be taken into account. Because of the narrow structure of the susceptibility spectrum (of the order of a few natural linewidths), the high-index effect will be washed out completely by Doppler broadening.

In the case of three-level systems, where atomic coher-

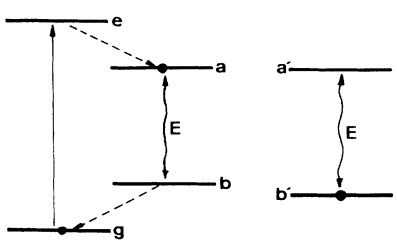

FIG. 29. Incoherent superposition of two two-level schemes with slightly different transition frequencies.

ence is present, the cancellation of absorption is insensitive to spatial fluctuations of the atomic density. Hence we can use atomic beams to avoid Doppler broadening. Moreover, there are certain schemes, such as the Raman-driven scheme, which are highly insensitive to Doppler broadening.

Furthermore, in order to mix the two kinds of two-level atoms evenly, we need collisions. However, the transition of the two species are very close so that collisions will tend to produce a rapid population exchange between the two kinds of atoms. The time between two successive collisions is of the order of 10^{-7} sec at 1 Torr and room temperature, which is of the same order as the radiative decay rate from the upper to the lower level of the optical transition. For an index of refraction of the order of 10, a much higher atomic density is necessary, which implies a much higher pressure unless the system is cooled. However, at low temperatures the fluctuations in N_1 and N_2 will become large leading to large fluctuations in χ''.

Finally, we note that in the two-level case, population inversion in one of the atomic species is required. In the phaseonium high-index material, of course, this is not the case. For these reasons a practical realization of a transparent high-index medium on the basis of an incoherent mixture of two-level atoms seems to be problematic.

VII. SUMMARY AND DISCUSSION

In the present paper we investigated various atomic systems that we consider as most appropriate to provide a high index of refraction while the absorption is small or, in principle, even vanishes. The underlying principles are quantum interference effects in a phaseonium gas. In a three-level system with dipole-allowed transitions from a single level to a pair of closely spaced levels, atomic coherence between the level pair causes interference terms in the total absorption and emission probability. Similar interference effects can occur if the lower or upper level of a single dipole-allowed transition is strongly coupled to another level, so that different absorption and/or emission pathways exist which may interfere.

Without population in the upper level(s) of the test-field transition, the coherence and interference effects lead to a large dip in the absorption spectrum, so that absorption can be canceled for particular values of the test-field frequency. At the same time the real part of the susceptibility vanishes. If, however, there is some population in the upper level, points of vanishing absorption and large real part of the susceptibility exists in the spectrum.

It is worth noting that χ' may have a positive or negative sign and hence $n^2=1+\chi'$ may become negative also. However, as explained in detail in Appendix B, the roots of this quadratic complex equation must be defined in such a way that the real part of the complex refractive index ($n=n'+in''$) is always positive.

At the beginning of our paper we introduced the simplest realization of a phaseonium gas, the case of injected atomic coherence. In Sec. II we discussed the establishment of atomic coherence via strong coherent fields applied simultaneously with the test field to the atomic system. We derived expressions for the real and imaginary part of the linear susceptibility for the cases of a microwave-driven upper- and lower-level doublet and a Raman-driven pair of lower states, and discussed the influence of coherence-diminishing processes such as Doppler broadening.

Comparing the two microwave schemes, the upper-level one turned out to be more favorable with respect to the maximum achievable value of the refractive index because of the fact that the off-diagonal decay rate of the forbidden transition c-a does not involve the strong decay rate of an allowed optical transition. On the other hand, in the lower-level scheme the coherence is less diminished by collisions. With regard to Doppler broadening, the achievable refractive index decreases strongly in both microwave cases except for very large values of the Rabi frequency Ω_μ, in which case, however, χ' is already small without Doppler broadening.

Among the schemes, we analyze the one most resistant to Doppler broadening and collisional effects is the Raman scheme. If the driving Raman field and the test field have the same propagation direction, both transitions experience a Doppler shift in the same direction. As a consequence the Raman scheme is less sensitive to Doppler broadening. The coherence produced between the lower levels is relatively insensitive to collisions. In contrast to the lower-level microwave case coherence does not require a difference in the zeroth-order populations of the two lower levels in the Raman scheme, an advantage for possible experimental implementation. The Raman scheme provides two other interesting features. In all other schemes high dispersion and vanishing absorption is achievable only for a definite test-field frequency. Moreover there is always a frequency region where the system shows gain. In the Raman scheme, however, nearly vanishing absorption and a high refractivity can be achieved over a broad spectral region. Furthermore, this is possible without having gain at any frequency.

In addition to the coherently driven schemes discussed in Sec. III, there are cases in which coherence or interference effects can be obtained by incoherent means. An interesting case from the theoretical point of view is the interference of radiative decays from two closely spaced levels with the same J and m_J quantum numbers to common ground levels. A practical realization of this decay interference, however, seems to be almost impossible in atomic systems. In addition, because of the narrow structures in the susceptibility spectrum, small Doppler broadening destroys the interference effects. The conditions for interference in radiative decays are so restrictive because the spontaneous transitions from the two upper levels need to share the same vacuum modes, which can have arbitrary polarizations.

These conditions become, however, unnecessary if the interference effect is created by an incoherent pump field of well-defined polarization. In this case, magnetic sublevels, for instance, may serve as the two levels and their spacing is limited only by the width of the pump field spectrum. In contrast to the interference between radiative decays, here we can generate upper- and lower-level

coherence by means of an incoherent driving field. The lower-level case is more advantageous with respect to collisions. However, both schemes are fairly sensitive to Doppler broadening, since the pump field is unaffected by the velocity distribution.

We would like to emphasize that we have considered in this paper only the linear response of the medium on the test field. Therefore the effect of the test field on the medium has been neglected—in contrast to the effect of the strong driving field. This is valid only for small test-field intensities. In particular, the Rabi frequency of the test-field transition has to be small compared to the radiative decay rate γ of this transition and small compared to the Rabi frequency of the driving field. Since for some applications of the high-index material larger test-field strengths are necessary, the nonlinear properties of the different schemes need to be investigated. This is planned to be the subject of a future publication [14].

ACKNOWLEDGMENT

This work was supported by the U.S. Office of Naval Research.

APPENDIX A: ULTRA-HIGH INDEX OF REFRACTION IN TWO TWO-LEVEL SCHEMES

Let us consider two kinds of two-level atoms as shown in Fig. 29. A probe field couples the transition a-b and a'-b' which have slightly different transition frequencies ω_1 and ω_2. Without the probe field, the first kind of atoms are most populated in a due to some pumping mechanism from level g to a via e, and the atoms of the second kind are in the ground state b'. We assume number densities N_1 and N_2 for the first and second kind of atoms.

The total polarization of the mixture is given by

$$P=N_1\wp_1\rho_{ab}+N_2\wp_2\rho_{a'b'}\ , \tag{A1}$$

where $\wp_{1/2}$ are the dipole matrix moments of the corresponding optical transitions, and ρ_{ab} and $\rho_{a'b'}$ are the off-diagonal matrix elements of the atomic density matrix for the corresponding transitions. The off-diagonal elements ρ_{ab} and $\rho_{a'b'}$ can be easily obtained from the steady-state solution of the equation of motion. We find for the susceptibility, $\chi=\chi'+i\chi''$:

$$\chi'=\frac{N_1'(\Delta-\omega_0)\wp_1^2/\epsilon_0}{[\gamma_{ab}^2+(\Delta-\omega_0)^2]+\gamma_{ab}G|\wp_1\mathcal{E}|^2/D}+\frac{N_2\wp_2^2(\omega_0+\Delta)/\epsilon_0}{[\gamma_{ab}^2+(\Delta+\omega_0)^2]+2\gamma_{ab}'|\wp_2\mathcal{E}|^2\Gamma_{a'b'}}\ , \tag{A2a}$$

$$\chi''=\frac{N_1'\gamma_{ab}\wp_1^2/\epsilon_0}{[\gamma_{ab}^2+(\Delta-\omega_0)^2]+\gamma_{ab}G|\wp_1\mathcal{E}|^2/D}+\frac{N_2\wp_2^2\gamma_{a'b'}/\epsilon_0}{[\gamma_{ab}^2+(\Delta+\omega_0)^2]+2\gamma_{ab}'|\wp_2\mathcal{E}|^2\Gamma_{a'b'}}\ , \tag{A2b}$$

with

$$N_1'=\frac{\Gamma_{ea}(\Gamma_{bg}-\Gamma_{ab})}{D}N_1\ , \tag{A3a}$$

$$G=2\Gamma_{ea}+\Gamma_{bg}\left[1+\frac{\Gamma_{ea}+\Gamma_{eg}}{R}\right]\ , \tag{A3b}$$

$$D=\Gamma_{ea}\Gamma_{ab}+\Gamma_{ea}\Gamma_{bg}+\Gamma_{bg}\Gamma_{ab}\left[1+\frac{\Gamma_{ea}+\Gamma_{eg}}{R}\right]\ , \tag{A3c}$$

$$\omega_0=\tfrac{1}{2}(\omega_{a'b'}-\omega_{ab})\ , \tag{A3d}$$

$$\Delta=\tfrac{1}{2}(\omega_{ab}+\omega_{a'b'})-\nu\ , \tag{A3e}$$

where $\Gamma_{\alpha,\beta}$ is the longitudinal decay rate from level α to level β; R is the pump rate from g to e; $\gamma_{\alpha\beta}$ is the transversal decay rate between α and β; and $|\mathcal{E}|^2$ is the intensity of the probe field. Note that N_1'/N_1 is usually only a few percent.

APPENDIX B: RELATION BETWEEN n AND χ

The linear response of an atomic system on an electric field E has been expressed by the complex susceptibility

$$\chi=\chi'+i\chi''\ . \tag{B1}$$

According to Eqs. (1), χ governs the relation between the test field E and the linear polarization P,

$$P(z,t)=\epsilon_0\int_{-\infty}^{\infty}d\tau[\chi'(\tau)+i\chi''(\tau)]E(z,t-\tau)\ , \tag{B2}$$

which appears as the driving term in the wave equation for the electric field:

$$\frac{\partial^2E}{\partial z^2}-\frac{1}{c^2}\frac{\partial^2E}{\partial t^2}=\mu_0\frac{\partial^2P}{\partial t^2}\ . \tag{B3}$$

The wave propagation in a linear medium can be described most conveniently in terms of the (complex) index of refraction n. Making a plane-wave ansatz for Eq. (B3),

$$E=E_0e^{i(\pm kz-\omega t)} \tag{B4}$$

with $\mathrm{Re}(k)\geq 0$ (the two different signs correspond to propagation in the positive or negative z direction), one obtains from (B2) and (B3) the dispersion relation

$$k^2-\frac{\omega^2}{c^2}n^2=0\ , \tag{B5}$$

where

$$n^2(\omega)=1+\chi(\omega)\ . \tag{B6}$$

As usual we set

$$k=\frac{\omega n}{c}\ . \tag{B7}$$

In order to have $\mathrm{Re}(k)\geq 0$ we have to choose the appropriate solution of the complex quadratic equation (B6). The square root maps two Riemann sheets of the complex χ plane on a single sheet. The branch cut is chosen along the negative χ' axis as indicated in Fig. 30, and the appropriate solution of Eq. (B6) can be expressed in terms of polar coordinates as

$$1+\chi=|1+\chi|e^{i\theta},\quad -\pi<\theta\leq\pi \tag{B8a}$$

$$n=(|1+\chi|)^{1/2}e^{i(\theta/2)}\ , \tag{B8b}$$

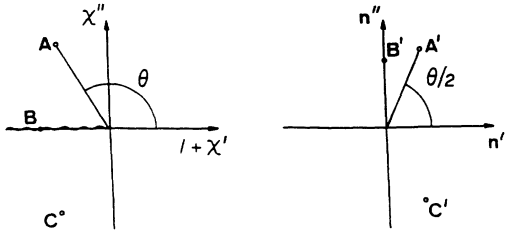

FIG. 30. The choice of a physically appropriate solution of Eq. (B6) corresponds to the definition of the branch cut in the two-sheet complex χ plane starting at $\chi=-1$ along the negative χ' axis. The points A, B, and C are mapped onto the points A', B', and C'.

where $\theta=0$ corresponds to the positive χ' axis. Note that points on the branch cut in the complex χ plane are mapped on the positive n'' axis. This choice can be most easily understood considering a medium in the half space $z\geq 0$ with $\chi'\leq -1$ and $\chi''=0$. A plane wave propagating in the positive z direction in a vacuum incident to the boundary of the medium at $z=0$ will be reflected. Inside the medium there is an evanescent exponentially decreasing field.

The solution of Eq. (B6) with the negative sign corresponds to

$$k=-\frac{\omega n}{c}\ , \tag{B9}$$

instead of (B7). Here, however, we use the common notation given in Eq. (B6). Using Cartesian coordinates, Eqs. (B8) can be written in the forms

$$n'=\left[\frac{[(1+\chi)^2+\chi''^2]^{1/2}+1+\chi'}{2}\right]^{1/2}\ , \tag{B10a}$$

$$n''=\left[\frac{[(1+\chi)^2+\chi''^2]^{1/2}-1-\chi'}{2}\right]^{1/2}\mathrm{sgn}(\chi'')\ , \tag{B10b}$$

with $\mathrm{sgn}(\chi'')=1$ for $\chi''=0$.

[1] G. Alzetta, A. Gozzini, L. Moi, and G. Orriols, Nuovo Cimento B **36**, 5 (1976); G. Alzetta, in *Coherence in Spectroscopy and Modern Physics,* edited by F. T. Arecchi, R. Bonifacio, and M. O. Scully (New York, 1978); G. Alzetta, L. Moi, and G. Orriols, Nuovo Cimento B **52**, 209 (1979).

[2] H. Gray, R. Whitley, and C. Stroud, Opt. Lett. **3**, 218 (1979); R. M. Whitely and C. R. Stroud, Phys. Rev. A **14**, 1498 (1976).

[3] S. Harris, Phys. Rev. Lett. **62**, 1022 (1989); A. Imamoğlu and S. Harris, Opt. Lett. **14**, 1344 (1989); A. Imamoğlu, Phys. Rev. A **40**, 2835 (1989); S. E. Harris, J. E. Field, and A. Imamoğlu, Phys. Rev. Lett. **64**, 1107 (1990); A. Imamoğlu, J. E. Field, and S. E. Harris, *ibid.* **66**, 1154 (1991); K. J. Boller, A. Imamoğlu, and S. E. Harris, *ibid.* **66**, 2593 (1991); J. E. Field, K. H. Hahn, and S. E. Harris, *ibid.* **67**, 3062 (1991).

[4] O. Kocharovskaya and Ya. I. Khanin, Pis'ma Zh. Eksp. Teor. Fiz. **48**, 581 (1988) [JETP Lett. **48**, 630 (1988)]; O. Kocharovskaya and P. Mandel, Phys. Rev. A **42**, 523 (1990); O. Kocharvskaya, P. Mandel, and S. Radeonychev, Phys. Rev. A **45**, 1997 (1992).

[5] M. O. Scully, S. Y. Zhu, and A. Gavrieliedes, Phys. Rev. Lett. **62**, 2813 (1989); M. O. Scully, in Proceedings of NATO Advanced Research Workshop on Noise and Chaos in Nonlinear Dynamical Systems, Torino, Italy, 1989.

[6] A. Lyras, X. Tang, P. Lambropoulos, and J. Zhang, Phys. Rev. A **40**, 4131 (1989); S. Basile and P. Lambropoulos, Opt. Commun. **78**, 163 (1990).

[7] J. Fontana and R. Pantell, J. Appl. Phys. **54**, 4285 (1983).

[8] M. O. Scully, Phys. Rev. Lett. **67**, 1855 (1991).

[9] M. O. Scully and Shi-Yao Zhu, Opt. Commun. **87**, 134 (1992).

[10] M. Fleischhauer, C. H. Keitel, M. O. Scully, and Chang Su, Opt. Commun. **87**, 109 (1992).

[11] M. Sargent III, M. O. Scully, and W. E. Lamb, Jr., *Laser Physics* (Addison-Wesley, Reading, MA, 1974).

[12] Here and in the remainder of the paper in all plots of the susceptibility a density of 1 atom per cm^3 is assumed. Therefore all results have to be multiplied by the number of atoms per cm^3.

[13] M. Fleischhauer, C. H. Keitel, L. M. Narducci, M. O. Scully, Shi-Yao Zhu, and M. S. Zubairy (unpublished).

[14] U. Rathe, M. Fleishhauer, Shi-Yao Zhu, and Marlan O. Scully (unpublished).